REPORT DOCUMENTATION PAGE

Form Approved OMB No. 0704-0188

Public reporting burden for this collection of information is estimated to average 1 hour per response, including the time for reviewing instructions, searching existing data sources, gathering and maintaining the data needed, and completing and reviewing the collection of information. Send comments regarding this burden estimate or any other aspect of this collection of information, including suggestions for reducing this burden to Washington Headquarters Services, Directorate for Information Operations and Reports, 1215 Jefferson Davis Highway, Suite 1204, Arlington, VA 22202-4302, and to the Office of Management and Budget, Paperwork Reduction Project (0704-0188), Washington, DC 20503.

1. AGENCY USE ONLY (Leave blank)	2. REPORT DATE	3. REPORT TYPE AND DATES COVERED
	August 1997	Final Report

4. TITLE AND SUBTITLE

Experimental and Theoretical Study of First Overtone Carbon Monoxide Laser Physics

5. FUNDING NUMBERS

F6170897W0081

6. AUTHOR(S)

Dr. Andre Ionin

7. PERFORMING ORGANIZATION NAME(S) AND ADDRESS(ES)

P. N. Lebedev Physical Institute
53 Leninsky Prospect
Moscow 117924
Russia

8. PERFORMING ORGANIZATION REPORT NUMBER

N/A

9. SPONSORING/MONITORING AGENCY NAME(S) AND ADDRESS(ES)

EOARD
PSC 802 BOX 14
FPO 09499-0200

10. SPONSORING/MONITORING AGENCY REPORT NUMBER

SPC 97-4014

11. SUPPLEMENTARY NOTES

12a. DISTRIBUTION/AVAILABILITY STATEMENT

Approved for public release; distribution is unlimited.

12b. DISTRIBUTION CODE

A

13. ABSTRACT (Maximum 200 words)

This report results from a contract tasking P. N. Lebedev Physical Institute as follows: The contractor will investigate the variation of specific input energy, gas density, gas temperature, pump pulse duration, and mixture on the operation of a CO laser operating on the first overtone. A comparison between the experimental and theoretical results will be made. In particular, laser output energy, efficiency, pulse duration and profile, and spectral content will be compared. All experimental and theoretical results will be presented in the final report with suggestions for improving the code and suggestions for further experiments.

DTIC QUALITY INSPECTED 4

14. SUBJECT TERMS

Lasers, Optical Components

15. NUMBER OF PAGES

50

16. PRICE CODE

N/A

17. SECURITY CLASSIFICATION OF REPORT	18. SECURITY CLASSIFICATION OF THIS PAGE	19. SECURITY CLASSIFICATION OF ABSTRACT	20. LIMITATION OF ABSTRACT
UNCLASSIFIED	UNCLASSIFIED	UNCLASSIFIED	UL

ГОСУДАРСТВЕННЫЙ НАУЧНЫЙ ЦЕНТР РОССИЙСКОЙ ФЕДЕРАЦИИ
ТРОИЦКИЙ ИНСТИТУТ ИННОВАЦИОННЫХ
И ТЕРМОЯДЕРНЫХ ИССЛЕДОВАНИЙ

**TROITSK INSTITUTE FOR
INNOVATION AND FUSION RESEARCH**

**РОССИЙСКАЯ АКАДЕМИЯ НАУК
RUSSIAN ACADEMY OF SCIENCES
P.N. LEBEDEV PHYSICS INSTITUTE**

Физический
ИНСТИТУТ
имени
П.Н.Лебедева
Ф И А Н

Experimental and Theoretical Study of First Overtone Carbon Monoxide Laser Physics

Scientific Report
Time period: March 1997-August 1997

The research work has been done in accordance with a special contract ***SPC-97-4014*** *with European Office of Aerospace Research and Development*

Scientific Leader

Prof. **A.Napartovich**

Dr. **A.Kurnosov**

Mr. **N.Turkin**

**Principal investigator,
Scientific Leader**

Prof. **A.Ionin**

Mr. **A.Kotkov**

Mr. **L.Seleznev**

Mr. **L.Afanas'ev**

Mr. **D.Sinitsyn**

Mr. **Y.Klimachev**

19970829 071

Moscow, 1997

Contents

1. Introduction

Carbon monoxide laser is a very attractive object both for practical applications and for fundamental research (Ionin et al, 1996a; Napartovich, 1996). From the practical point of view its high output efficiency (up to 50%) and a possibility of an achievement of high average power (~0.1-1.0 MW) are very important. For the fundamental research CO molecule is an excellent example of an anharmonic oscillator. Just because of basic properties of the anharmonic oscillator an inversion population between vibrational-rotational levels of CO molecule is created by vibration-vibration exchange and lasing itself is possible not only in fundamental band (FB) (V→V-1; λ~4.9-7.0 μm) but in the first overtone (FO) spectral band also (V→V-2; λ~2.5-4.0 μm). The latter spectral band is very promising one for practical applications such as atmosphere monitoring, laser radar, spectroscopy etc.

For the first time FO lasing was experimentally observed in (Bergman et al, 1977) for electric discharge supersonic CO laser in 2.7-3.1 μm spectral region, output power and laser efficiency being 20 W and 0.6%. Total output power on FO and FB was 88 W. Application of e-beam controlled discharge (EBCD) pumping technique gave an opportunity to increase FO CO laser efficiency up to 3% (Basov et al, 1978). There are only a few papers where characteristics of FO CO laser have been studied experimentally (Basov et al, 1980a,b, 1985; Gromoll-Bohle et al, 1989; Bachem et al, 1993; Belykh et al, 1994, 1995). The maximum output energy and laser efficiency for EBCD FO CO laser comes up to 50 J and 5% (Basov et al, 1985). FO CO lasing was observed within 2500-3800 cm^{-1} spectral region, lasing on 37-35 vibrational transition being demonstrated (Bachem et al, 1993).

Theoretically the possibility to achieve lasing in the overtone band of CO laser has been predicted in (Konev et al, 1977). The analytical theory of the steady state operation of the FO CO laser was developed in (Zhdanok et al, 1980). In (Konev et al, 1981) numerical studies were performed on simultaneous lasing in fundamental and overtone bands. It was found that suppression of lasing in the FB strongly improves characteristics of the FO CO laser. The most detailed model and numerical studies of the FO CO laser in comparison with an experiment were published in (Belykh et al, 1994, 1995). Practically no comparison has been done earlier between the theory and experiment except for (Belykh et al, 1994, 1995), where the experimental possibilities were very restricted resulting in comparatively low laser efficiency (not higher than ~1%).

The objective of the research work is a comparison between the theory developed for real experimental conditions and experimental results on the FO CO laser aimed at looking for possible ways of increasing the laser efficiency. Resulting from the comparison some modifications of the theory and additional measurements are anticipated. In as much as FB lasing both spoils FO laser characteristics (as was pointed out earlier (Basov et al, 1980a,b, 1985); (Konev et al, 1981)) and also makes the comparison between theory and experiment much more complicated, the special measures were undertaken for its suppressing.

2. Description of a basic theoretical model

Generally, one may assume that for description of the FO CO laser the mathematical model of CO laser operating in the fundamental band is applicable. However, up to nowadays the model for the FB CO laser can not be blindly trusted. Some unresolved problems still remain in modeling the FB CO laser (Napartovich, 1996). For efficient operation of the FO CO laser the laser mixture should be excited up to higher vibrational levels than it is sufficient for successful operation of the FB CO laser. In this situation the role of processes in which the molecules on high vibrational levels and excited electronic levels are involved grows. Information about such processes is much more scarce, and a strong scatter in data exists. Therefore, formulation of the numerical model of the FO CO laser and its verification by experiments is non trivial problem. Our previous attempt of description of the FO CO laser excited by a short discharge pulse (Belykh et al, 1994, 1995) may be considered as an encouraging one. In this report we start from the model (Belykh et al, 1994, 1995) giving more details about it. Then, in the section 5, after comparison of theoretical predictions with experimental data obtained at Lebedev Physics Institute the conclusions are made about directions in which the kinetic model should be modified.

2.1. Governing processes and basic equations

The mechanism of formation of a partial inversion between rotation-vibrational levels in CO molecule is very specific. The key process is so called anharmonic pumping resulting from the vibration-vibration (V-V) exchange between molecules on low and high vibrational levels. Because of anharmonicity of molecular vibrations the vibrational quantum diminishes with the level number. Then at a low gas temperature the more probable is the process where the molecule on a lower level comes down and on the higher level comes up. The necessary conditions this process to prevail against the reverse one are: $Q_{VV} >> Q_{VT}$, and $T_v > T$, where Q_{VV} and Q_{VT} are the rates of the V-V exchange and V-T (vibration-translation) relaxation, respectively, T is the gas temperature, and T_v is the effective vibrational temperature for lower levels. The resulting evolution of the vibrational distribution function (VDF) after the discharge was switched on is shown schematically in **Fig.**2.1. (An analytical theory giving explicit expressions for the VDF shape as a function of time was formulated in (Zhdanok et al, 1979)). As one can see from **Fig.**2.1, the effective vibrational temperature describing the relative populations on the neighboring levels is very high in the range of $v \geq 10$. For this particular case (generally, for v greater than the so-called Treanor number (Treanor et al, 1968)), in this range the inversion may be realized between rotational sublevels in adjacent vibrational bands. It is clear that the inversion takes place simultaneously on many transitions. This is the underlying reason for multifrequency lasing in the FB CO laser.

When lasing in the fundamental band is suppressed the same mechanism produces the partial inversion on the first overtone transitions. Comparing spontaneous emission probabilities for fundamental and first overtone bands shown in **Fig.**2.2 it becomes clear that overtone lasing may take place on

transitions higher than for the fundamental band. It means that the model of the FO CO laser should meet a requirement to describe with reasonable accuracy highly excited gas.

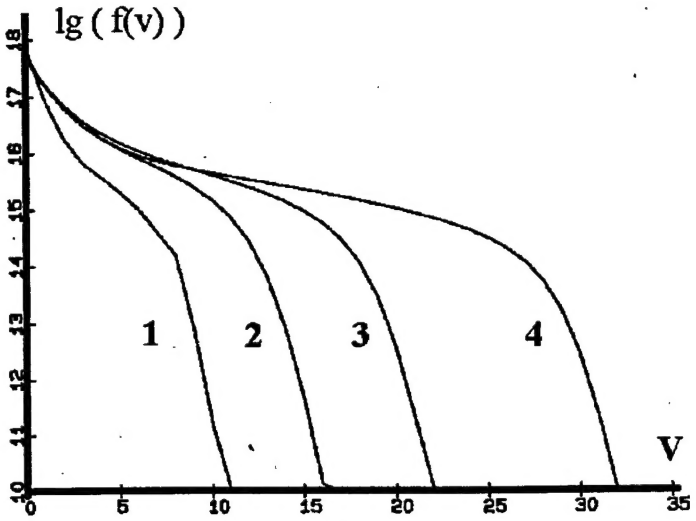

Fig.2.1. Time evolution of VDF for CO molecules.

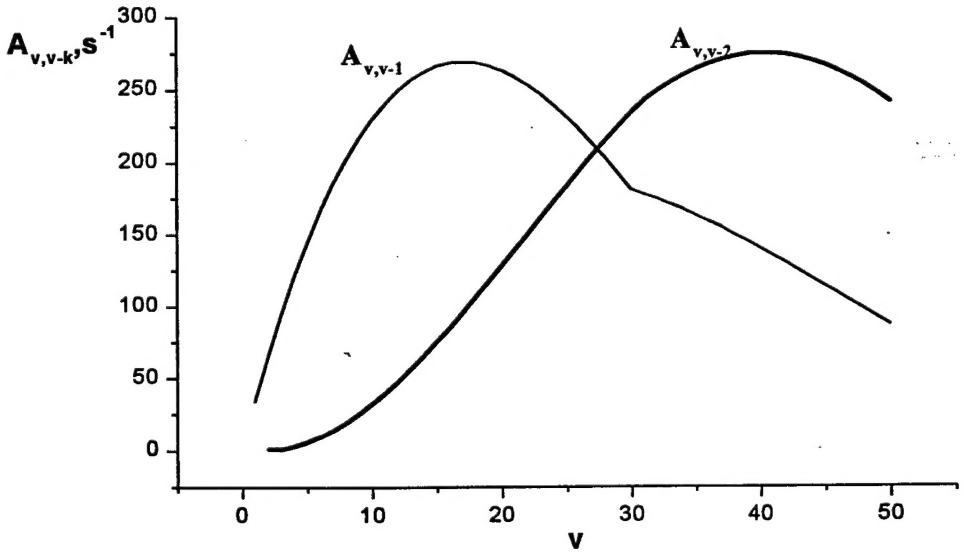

Fig.2.2. Einstein coefficients for fundamental band and first overtone band emissions

The mathematical model of the CO overtone laser was formed by a system of kinetic equations describing the temporal evolution of populations of vibrational levels of molecules CO and N_2. Schematically, this system has a form:

$$\frac{dn_v}{dt} = R^v_{e-V} + R^v_{VV} + R^v_{VT} + R^v_{SP} + g_{v+2,i} I_{v+2,i} - g_{v,i+1} I_{v,i+1}. \qquad (2.1)$$

Here $R^v_{e-V}, R^v_{VV}, R^v_{VT}, R^v_{SP}, g_{v+2,i} I_{v+2,i}$ are the rates of change of the population of the v-th level in the excitation/quenching processes in collisions with plasma electrons, the vibration-vibration exchange processes, the vibrational relaxation processes and the spontaneous and stimulated emission processes. Correspondingly $I_{v,j}$ is the laser intensity, $g_{v,j}$ is the gain for transitions in the first vibrational overtone. The intensities $I_{v,j}$ were found by solving the following equations:

$$\frac{dI_{v,i}}{dt} = c(g_{v,i} - \Gamma_{v,i})I_{v,i} + \frac{L\Omega}{4\pi n_v} A^{v,v-2}, \tag{2.2}$$

where c is the speed of light, L is the cavity length, Ω is the limiting resonator aperture, $\Gamma_{v,i}$ is the threshold gain coefficient for the given transition, $A^{v,v-2}$ is the relevant Einstein coefficient.

The electron energy distribution function (EEDF) at high degrees of vibrational excitation depends not only on E/N (E is the electric field strength, N is the gas density), but also on the degree of vibrational excitation. Therefore, in our model the steady-state Boltzmann equation for the spherically symmetric part of the EEDF was computed simultaneously with systems (2.1) and (2.2). Schematically, the electron Boltzmann equation has a form:

$$\frac{dJ_F(u)}{du} + \frac{dJ_{el}(u)}{du} = St(f_0), \tag{2.3}$$

where u is the electron energy; J_F and J_{el} are the electron fluxes in the energy space, which appear because of the presence of an electric field and because of elastic losses and excitation of rotational levels; $St(f_0)$ is the inelastic collision integral, including the excitation of vibrational and electronic levels and transitions between vibrational excited levels.

We solved also the equation for the gas temperature:

$$NC_V \frac{dT}{dt} = W_{VV} + W_{VT} + W_*, \tag{2.4}$$

where $W_{VV} + W_{VT} + W_*$ are, respectively, the amounts of the heat released in the VV exchange, VT-relaxation processes, and direct heating of the active medium in the discharge by elastic and inelastic (involving excitation of molecular rotation) collisions with electrons; C_v is the specific heat capacity at a constant volume. The heating rate, W_* should be found by solving the Boltzmann equation for the EEDF in dependence on the mixture composition, parameter E/N, and vibrational distribution function. However, in practical numerical simulation of CO laser it is usual to treat W_*, as a fit parameter, allowing to reach a good agreement of the theory with an experiment. As was shown earlier, the attempts to find W_* by solving the Boltzmann equation overestimate considerably the energy efficiency of lasing compared with the measured values. We assumed that $W_* = 0.15W$ (W is the specific electric discharge power) and it is close to experimentally measured values at $E/N \approx 10^{-16}$ V cm^2 for CO-N_2 mixtures and for pure CO. Thus we solved the Boltzmann equation only to specify the distribution of vibrational excitation rate between various vibrational levels of CO and N_2 molecules.

2.2. Choice of kinetic parameters

2.2.1. V-V exchange coefficients

As it was mentioned above, the V-V exchange is a key process realising self-pumping of high vibrational levels in the excited gas of diatomic molecules like CO or N_2. It means that a correct choice of kinetic coefficients characterising the V-V exchange is of particular importance. In reality, knowledge of all necessary kinetic coefficients is far from to be complete. First of all, widely used model where only single-quantum exchange processes are left is quite questionable for description of populations of vibrational levels with numbers exceeding 15. As it will be shown below, this is the range where overtone transitions have partial inversion and relatively high small signal gain. Applicability of the approximation of the single-quantum V-V exchange processes in the theory of the FO CO laser should be checked separately. Because of quite a few experimental data about dynamics of the vibrational distribution function for high levels this problem has no ideal solution at present. Unfortunately, existing quantum-mechanical theory of these processes (Billing et al, 1983) is not quite reliable and needs to be verified by experiments.

In this report, we restrict ourselves by using the traditional model for V-V exchange processes taking into account only single-quantum processes. Our choice of kinetic coefficients is based on analysis made in (Kochetov, 1976).

In particular, V-V exchange rate coefficient $k_{v,v-1}^{v',v'+1}$ for the process

$$CO(v) + CO(v') \rightarrow C)(v\text{-}1) + C)(v'+1)$$

with an energy defect $\Delta E_{v,v'}$ was calculated in the following manner.

For collisions where the ground-state molecule takes place and $\Delta E_{v,0} \le 10\ (T(K))^{1/2}$ cm^{-1} the rate coefficient was calculated using an expression:

$$k_{v,v-1}{}^{0,1} = v \cdot z \cdot (0.919 \cdot T^{-1} + 61.9 \cdot T^{-2}) \cdot \exp[-(0.188 \cdot \Delta E_{v,0} \cdot T^{-1/2})^2], \qquad (2.5)$$

where the gas collision frequency is equal to $z = 1.73 \cdot 10^{-11}\ T^{1/2}$ cm^3 s^{-1}. For other $v \le 15$ which did not satisfy to the above condition the averaged experimental data were used at the gas temperature values T = 100; 300; 500 K. For the intermediate values of temperature the interpolation was used:

$$\ln(k^{0,1}{}_{v,v-1})_T = \ln(k^{0,1}{}_{v,v-1})_{T1} + \frac{(\ln(k^{0,1}{}_{v,v-1})_{T_2} - \ln(k^{0,1}{}_{v,v-1})_{T1})}{T_2 - T_1} \cdot (T - T_1) \qquad (2.6)$$

For greater $v \ge 15$ the rate coefficient $k_{v,v-1}^{0,1}$ was calculated by Herzfeld formula (Herzfeld et al, 1959):

$$k^{v',v'+1}{}_{v,v-1} = |q_{v,v-1}|^2 \cdot |q_{v'+1,v'}|^2 \cdot T \cdot S_{1,0} \cdot \exp[(Ev + Ev' - Ev - 1 - Ev' + 1)/(2 \cdot k \cdot T)] \cdot f(y_{v,v'}); \qquad (2.7)$$

where

$$y_{v,v'} = \frac{\delta}{\sqrt{2}} \cdot \left(\frac{\Theta}{T}\right)^{1/2} \cdot |v-(v'+1)|; \quad \Theta = 4.45 \cdot 10^6 K; \quad S_{1,0} = 5 \cdot 10^{-16}; \quad |q_{v,v-1}|^2 = v \cdot (1-\delta)/(1-\delta \cdot v);$$

$$f(x) = 8.2x^{7/2} \exp(-3x^{2/3}), \qquad \text{at } x \geq 20$$

$$f(x) = 0.5(3 - \exp(-2x/3)), \qquad \text{at } x < 20.$$

General rate coefficient $k_{v,v-1}^{v',v'+1}$ was calculated according to

$$k^{v',v'+1}{}_{v,v-1} = \left|\frac{q_{v,v-1}}{q_{1,0}}\right|^2 \cdot \left|\frac{q^{v'+1,v'}}{q_{1,0}}\right|^2 \cdot \left|\frac{q_{1,0}}{q_{v-v',v-v'-1}}\right|^2 \cdot k^{0,1}{}_{v-v',v-v'-1}.$$

The rate coefficients for reverse processes were calculated from the detailed balance:

$$k^{v',v'+1}{}_{v,v-1} = k^{v-1,v}{}_{v'+1,v'} \cdot \exp\left(2 \cdot \delta \cdot E_0 \cdot (1+v'-v)/kT\right).$$

In a number of articles all the elements of the matrix of V-V exchange coefficients were calculated for a broad temperature range using an unified analytical approximation of a modified SSH-theory, in which an input of both short-range and long-range molecular forces was included (Smith et al, 1976; Stanton et al, 1980; Flament et al, 1992). Contrary to described above methodology, using of the unified theory does not allow one to describe with a reasonable accuracy experimental data for the temperature range 100-500 *K*. This fact was noticed also in (Stanton et al, 1980). For typical conditions of the FB CO laser our special tests demonstrated that a difference in the laser characteristics induced by differences in V-V exchange rate coefficient sets is insignificant and may be ignored.

The V-V' exchange between CO and N_2 molecules on the lower levels is characterised by a relatively big energy defect ($\Delta E \approx 200$ cm^{-1}). Therefore the effect of a multi-pole interaction between molecules was neglected in (Rapp et al, 1964; Shin et al, 1977). However, an analysis of the numerical data obtained in (Mastrocinque et al, 1976) using the Sharma-Brau theory (Sharma et al, 1969) and in semi-classical calculations (Billing, 1980) allows us to make a conclusion that for $\Delta E \leq 100$ cm^{-1} the multi-pole interactions are dominant in V-V' exchange. Their input at $\Delta E \approx 200$ cm^{-1} is less about an order of magnitude and becomes comparable with short repulsive interactions. Therefore we calculated these rate coefficients according to modified SSH-theory where both type of interactions were taken into account. A part due to short-range interactions was described by a formula:

$$^{S}K^{v',v'+1}{}_{v,v-1} = a \cdot z \cdot T \cdot \frac{v}{(1-v\cdot\delta)} \cdot \frac{(v'+1)}{(1-(v'+1)\cdot\delta)} \cdot \exp\left(\frac{\Delta E}{2\cdot T}\right) \cdot f(y(\Delta E, T)) \cdot F; \qquad (2.8)$$

where $a = 6.61\ 10^{-8}\ K^{-1}$, $z = (\pi\sigma^2/4)\ V_M$ is gas kinetic collision frequency, V_M is the average relative translational velocity, $f(y)$ is an adiabatic factor (Smith et al, 1976):

$$f(y) = \begin{cases} 0.5 \cdot \exp(-2y/3) \cdot (3 - \exp(-2y/3)); & 0 \le y \le 21.622; \\ 8 \cdot (\pi/3)^{1/2} \cdot y^{7/3} \cdot \exp(-3 \cdot y^{2/3}); & y \ge 21.622; \end{cases}$$

The adiabatic factor accounts for attractive part of inter-molecular interaction.

For description of the long-range interactions the analytical approximation of (Rockwood et al, 1973) was used:

$$^{L}K^{v',v'+1}_{v,v-1} = b \cdot z \cdot \frac{1}{T} \cdot \frac{v}{(1 - v \cdot \delta)} \cdot \langle v'+1|q|v' \rangle^2 \cdot \exp\left(\frac{\Delta E}{2 \cdot T}\right) \cdot \exp\left(-\frac{\Delta E^2}{T \cdot c}\right); \qquad (2.9)$$

which produced results agreeing with calculations by Sharma-Brau theory within (10-30)%. Here $b = 4\ 10^{-2}\ K$, $c = 145\ K$, $\langle v' + 1|q|v' \rangle$ is the matrix element of quadruple moment of a nitrogen molecule between vibrational wave functions. The total V-V' exchange rate coefficient was calculated according to the formula:

$$k^{v_i,v'+1}_{v,v-1} = {}^{S}K^{v',v'+1}_{v,v-1} + {}^{L}K^{v,,v'+}_{1v,v-1}.$$

Empirical coefficients a, b, c were derived by treating detailed experimental data in (Allen et al, 1980), where the V-V' exchange coefficients were measured for CO and N_2 $k^{0,1}_{1,0}$ for the gas temperature range 80-300 K for three isotopes of nitrogen molecules: $^{28}N_2; ^{29}N_2; ^{30}N_2$. The V-V exchange defect energy was varied from one isotope to another.

The V-V exchange coefficients for nitrogen molecules were computed according to Egn. (2.8). Because of some scatter in experimental data at the room temperature and the lack of these data for low temperatures we used the results of calculations in (Billing et al, 1979). For the magnitude of the empirical coefficient a in (2.8), $a = 4.11\ 10^{-8}\ K^{-1}$ a reasonable agreement is achieved between the approximation (2.8) and the numerical results (Billing et al, 1979) for the reactions $N_2(v) + N_2(1) \rightarrow N_2(v+1) + N_2(0)$ for $v \ge 1$.

2.2.2. V-T relaxation coefficients

For the description of the rate coefficients for V-T relaxation processes taking place in collisions between vibrational excited molecule and a partner which may be CO or N_2 molecule or He atom the approximation (2.8) again was used. The empirical coefficients were taken from (Smith et al, 1976) for CO and N_2 partners, and for He atoms the results of the experimental measurements in (Andrews et al, 1984) were treated to extract these coefficients.

2.2.3. Spectroscopic constants

The gain coefficient for the FO CO laser transitions were calculated according to the well known formula (Patel, 1964):

$$g_{v+2,v} = (\lambda^2/8\pi)\, A_{v+2,v}\, S_J\, [N_{v+2}\frac{B_{v+2}}{kT}\exp(-\frac{B_{v+2}F(J\pm 1)}{kT}) - N_v\frac{B_v}{kT}\exp(-\frac{B_v F(J)}{kT})]\, G(\lambda), \quad (2.10)$$

where $S_J = J$ for P-branch, and $S_J = J + 1$ for R-branch transitions, $F(J) = J\,(J + 1)$, the sign "+" should be tāken for R-branch and "-" for the P-branch transitions, $A_{v+2,v}$ is the spontaneous emission probability, λ is the wavelength, $G(\lambda)$ is a normalised spectral line profile. The laser transition frequencies were calculated using the empirical approximation derived in (Guelachvili et al, 1983). Frequencies calculated by this approximation agree very well with experimental measurements in (Bachem et al, 1993)

The normalised spectral line profile was approximated by an integral including Lorentz shape and Doppler mechanism of line broadening (Penner, 1959):

$$G(\lambda) = (4\ln 2/\pi)^{1/2} H(b)/\Delta\nu_D$$

$$H(b) = \frac{b}{\pi}\int_{-\infty}^{\infty}\frac{\exp(-z^2)}{z^2+b^2}dz = [1-\Phi(b)]\exp b^2,$$

$$\Phi(b) = \frac{2}{\pi}\int_0^b \exp(-x^2)dx,\ b = \frac{\Delta\nu_l}{\Delta\nu_D}\sqrt{\ln 2},$$

$\Delta\nu_l$, $\Delta\nu_D$ are collision and Doppler widths respectively. The Doppler width is defined by a well known expression: $\Delta\nu_D = \nu/c\sqrt{8\ln 2kT/M}$, and the collision width by $\Delta\nu_l = 2\ \Sigma\gamma_i\ p_i$, where p_i is the partial pressure of gas components, γ_i is a half width of the considered spectral line induced by collisions of CO molecule with i-th gas component particles. For CO-CO and CO-N_2 collisions this half width is approximated by a formula (Kochetov, 1976): $\gamma^{(m)} = \gamma^{(m)}_{300}(\frac{300}{T})^{0.7}$, where m is the number of the rotational sub-level for the selected transition. The quantity $\gamma^{(m)}_{300}$ was taken from the work (Hunt et al, 1968) for CO-CO collisions at m = 1-21. For higher values of m = 22-30 and for collisions of CO molecules with N_2 the magnitudes of $\gamma^{(m)}_{300}$ were taken from (Bounich et al, 1973). For CO-He collisions the temperature dependence of the correspondent half width was approximated by a formula $\gamma^{(m)} = \gamma^{(m)}_{300}(\frac{300}{T})^{0.5}$, where the magnitudes of $\gamma^{(m)}_{300}$ were tabulated in (Andrews et al, 1975). The rotational constants for CO molecules were approximated by an expression:

$$B_v = B_e - \alpha_e\,(v + \tfrac{1}{2}) + \gamma_e\,(v + \tfrac{1}{2})^2 - D_e\,(J + 1)J + \beta_e\,(v + \tfrac{1}{2})J(J + 1),$$

where B_e= 1.931271 cm^{-1}; α_e= 0.017513 cm^{-1}; γ_e= 2.96 10^{-6} cm^{-1}; D_e= 6.1198 10^{-6} cm^{-1}; β_e= 0.9876 10^{-9} cm^{-1}.

The spontaneous emission probabilities $A_{v,\,v\text{-}k}$ for v = 1-30 and k = 1-5 are collected in the work (Rockwood et al, 1973). For higher vibrational levels $v \geq 30$ these probabilities were calculated in (Kochetov, 1976). **Fig.**2.2 shows these probabilities for fundamental and overtone bands. Recently the

comparison was made between those shown in **Fig.**2.2 and results of measurements published in (Lightman et al, 1978) and (Farrenq et al, 1985). Differences do not exceed 10%.

2.2.4. Electron scattering cross sections

For typical conditions of EBCD in mixtures of the CO laser the value of the parameter E/N falls in the range where electrons excite quite effectively vibrations of molecules, and excitation of electronic levels, dissociation and ionization of molecules may be neglected. As it was mentioned above, despite the good knowledge of electron scattering cross sections from 'cold' N_2 and CO in our model the additional fit parameter was introduced allowing for removing discrepancies between theory and experiment for the FB CO laser. Under the term 'cold' we mean molecules in ground vibrational state. Unfortunately, any experimental data about electron scattering from vibrational excited molecules do not exist. Therefore it is necessary to use some of the theories of collisions between electrons and molecules verifying it by comparison with experimental data for excitation of molecular vibrations from the ground state. The experimental data on electron impact excitation of molecules N_2 (**Fig.**2.3) and CO (**Fig.**2.4) are known up to the transition 0→8 (Schulz, 1979). Accuracy of these data is considered usually as a high enough. In fact, we need to know all the elements of a matrix consisted of cross sections for electron impact induced transitions $v \rightarrow v + k$. To calculate all the remaining cross sections we applied theoretical approximations derived by (Aleksandrov et al, 1978) for N_2 and (Aleksandrov et al, 1979) for CO. To evaluate the level of accuracy of the theoretical approximations, the calculated cross sections as a function of electron energy are compared with experimental data (Schulz, 1979) in **Figs.**2.5 and 2.6. One can see that in both cases the theory underestimates the magnitude of cross sections at higher electron energies. At present, several theoretical calculations are known producing the necessary set of cross sections. One of the problems for a future is to study the sensitivity of the FO CO laser characteristics to the choice of a specific model for electron-molecule collisions with formation of resonance unstable (transient) ion. As it is well known, exactly this mechanism is the dominant one in processes of vibrational excitation of CO and N_2 by electron impact.

2.3. Adaptation of the model to the experimental conditions

When comparing results of theoretical simulations with experimental data a care should be taken that the parameters entering the model closely correspond to the experimental ones. To solve this problem joint efforts should be made by both an experimenter and a theorist. The mathematical model replaces a real three-dimensional device by a point-like object assuming uniform distributions of discharge characteristics over the fixed space. Instead of modeling real propagation of the laser beams within the cavity the simplified purely dynamic equation (2.2) is solved. For experimental conditions errors introduced by these approximations may be considered as not very serious: estimations gave the level of the error of (10-20)%. The same level of accuracy should be kept when parameters of the theory are fitted to the experiment.

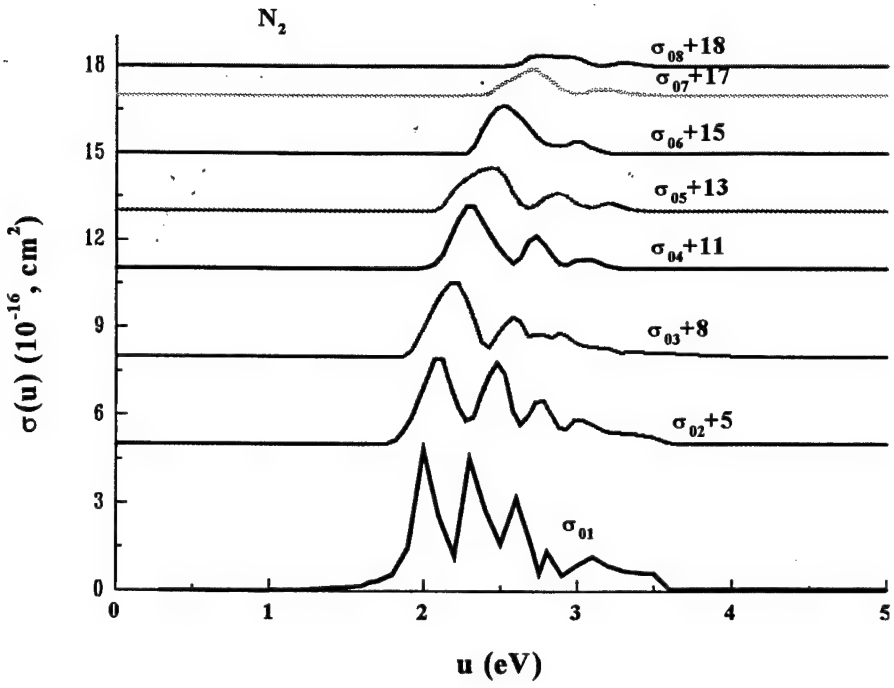

Fig.2.3. Experimental (Schulz, 1979) cross sections for excitation of vibrational levels of N_2 from the ground state

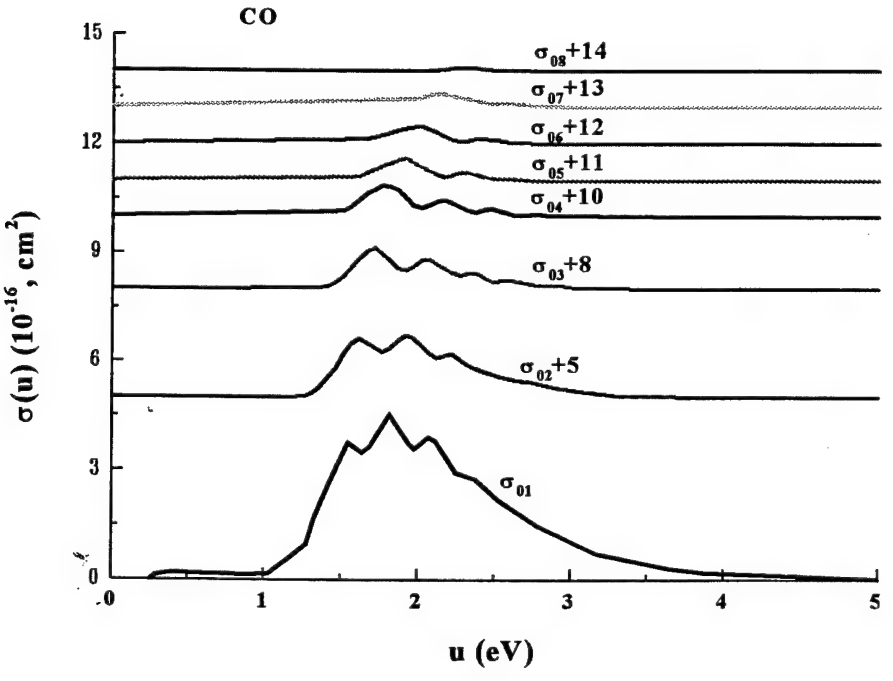

Fig.2.4. Experimental (Schulz, 1979) cross sections for excitation of vibrational levels of CO from the ground state.

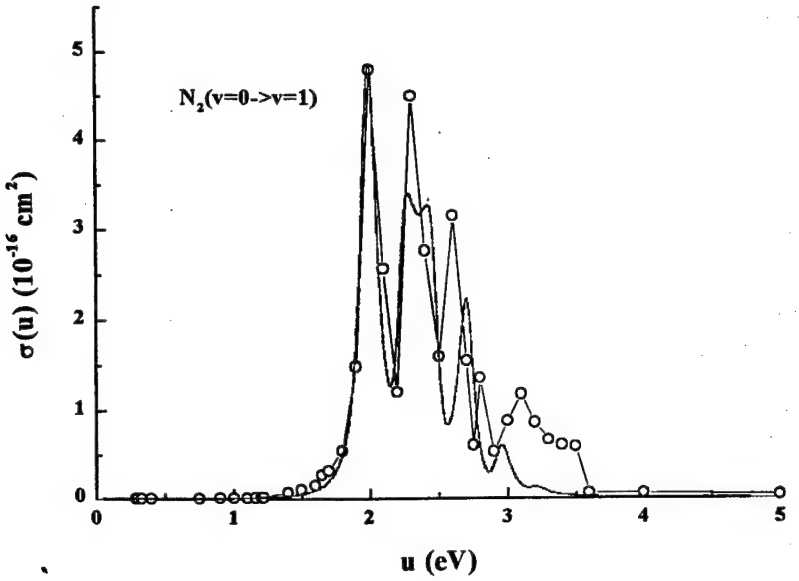

Fig.2.5. Comparison of experimental (Schulz, 1979) and calculated (Aleksandrov et al, 1979) cross sections for excitation of N_2 molecule by electron impact: v=0→v=1

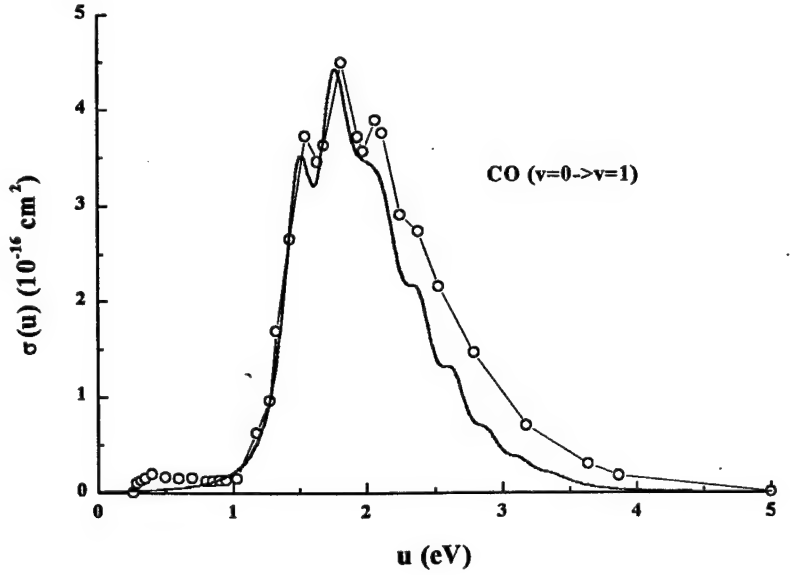

Fig.2.6. Comparison of experimental (Schulz, 1979) and calculated (Aleksandrov et al, 1979) cross sections for excitation of CO molecule by electron impact: v=0→v=1

The parameters of the model may be divided into two groups:

1. Characterizing the discharge;
2. Characterizing the laser cavity.

1. In experiments (see section 3), the gas mixture excited by EBCD occupied the volume with the discharge gap length 9 cm, the discharge width 16 cm and its length 120 cm. However, only 1/9 of the volume corresponds to the region where from the laser power was extracted. Within this region, p[illegible]ma

parameters are uniformly distributed provided the electron-beam gun operates properly. Then we may apply 0-D model for description of the experiments. In our model two governing parameters taken from the experiment are involved: the reduced electric field strength, *E/N* and the discharge power density as a function of time. Variations of the gas density during the laser pulse were neglected (the total volume was restricted by electrodes and side walls preventing from the gas expansion). The electric field was calculated from the time dependent voltage in an assumption of uniform distribution along the discharge gap. The typical time dependence of the reduced electric field strength (*E/N*) is shown in **Fig.**2.7 for the experimental conditions described in the figure option. The discharge current, I was measured in experiments, and the power density was calculated as a product of E and $j = I / S$, where S is the electrode area. The resulting time dependence of the specific discharge power is shown in **Fig.**2.8 for the same conditions as in **Fig.**2.7.

One of possible sources of an error when comparing results of 0-D model simulations with experiments is an existence of non-uniformity in plasma parameters along the optical axis. They may be induced by fluctuations of the e-beam current density. This problem requires a special study.

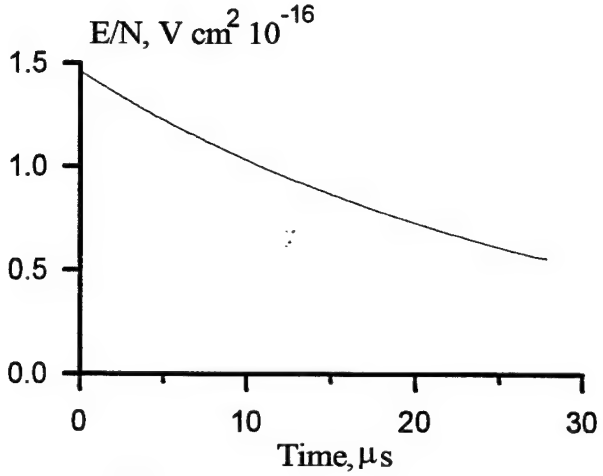

Fig.2.7. Typical time dependence of reduced electric field strength in discharge:
$CO:N_2 = 1:9$;
$N = 0.3$ Amagat;
$T_0 = 105$ K;
$Q_{in} = 364$J/l Amagat;
discharge current duration 28 μs

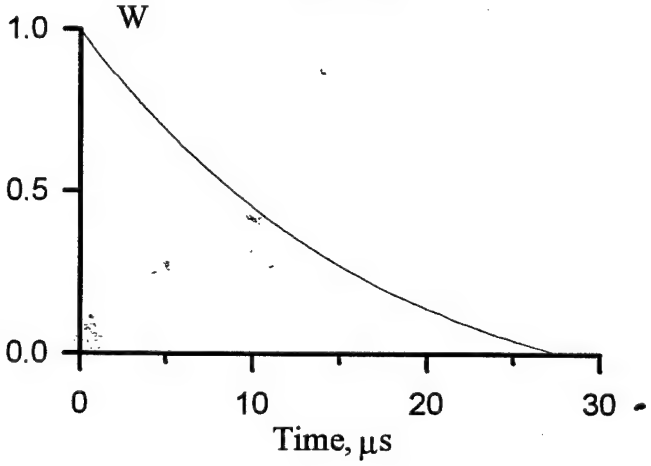

Fig.2.8. Typical time dependence of specific input power W(t) used in calculations (conditions are the same as in **Fig.**2.7)

2. An accurate characterization of the laser cavity is of a particular value to achieve a good correlation between theory and experiment. In our model the laser cavity was described in the simplest approximation of radiation intensity balance inside the laser cavity for each lasing transition. The following parameters were measured in experiment and used in the model: the cavity round trip time; spectral transmittance and refractive index of the spectral filter employed for suppression of the fundamental band lasing; scattering and absorption losses in metal mirrors and in the Brewster window. The laser beam size was governed by the diaphragm situated near the plane mirror (see **Fig.**3.1). The output coupling realised by reflection from the declined selective filter plate was calculated as a function of the decline angle and radiation frequency using Fresnel formulae. An overall cavity loss including useless losses and output coupling loss also was calculated using the above listed quantities. The resulting calculated overall cavity loss is shown in **Fig.**2.9 for overtone transitions starting from the vibrational level v at a fixed quantum rotational number $J = 12$. This dependence was calculated for the filter plate declined at the angle 33°. The strong increase of the losses for the transitions higher than 28→26 evidently restricts the laser spectrum from the long wavelenghts side.

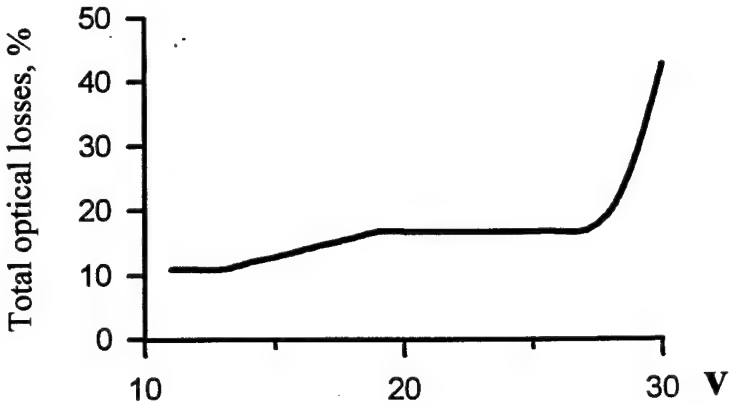

Fig.2. 9. Overall loss of resonator vs the number of upper level for overtone transitions v→v-2 used for simulations of laser characteristics (The beam incidence angle onto the filter plate is equal to 33°)

3. Experimental research of FO CO laser

3.1. Laser installation and optical scheme of the experiments

3.1.1. EBCD CO laser installation

The experimental research of characteristics of FO CO laser with suppressed FB lasing has been carried out on cryogenically cooled EBCD laser installation detailed description of which can be seen in (Ionin et al, 1996b). The active medium length L_{am} was 1.2 m, EBCD volume 18 litres, electrical discharge gap 9 cm. Maximum e-beam density in EBCD volume was ~20 mA/cm^2, maximum electron energy being 150 keV. By changing the heating of the thermoionic cathode of e-gun we changed e-beam current pulse length, and, hence, the pulse length of EBCD current within the range of 25 - 1500 μs. e-Beam current pulse had a triangular shape with a maximum on its front. Practically, EBCD current had the same shape. A capacity of capacity bank varied from 12 up to 65 μF, although in the most of the experiments it was 33 μF. The specific input energy (SIE) varied from 50 up to 500 J/l Amagat. Gas temperature changed between 100 and 300 K. Maximum gas density came up to 0.5 Amagat (Amagat is a gas density unit corresponding to the number of moles in a mole volume, 22.4 liter).

3.1.2. Measuring equipment

An output energy was measured by thermoelectric calorimeter IMO-2 (measuring limits 0.1 mJ - 10 J). When measuring output energy higher than 10 J, calibrated attenuators were used. Time-history of e-beam and EBCD currents was measured by low-inductance resistor. Time-history of laser output was detected by Ge:Au photodetector with response time of ~ 0.8 μs. For measuring the shape and duration of the laser pulse, EBCD current etc. the oscilloscope C8-14 was used. The spectral characteristics of laser radiation were detected by home-made spectrograph using diffraction grating (150 lines/mm). The output energy spectral distribution was detected by thermosensibile paper (carbon paper) placed in a focal plane of the spectrograph. The spectral features of optical elements (laser mirrors, spectral filters etc.) were measured by spectrophotometer "PERKIN-ELMER- 983G."

3.1.3. Optical scheme of FO CO laser resonator

The optical scheme of the laser resonator used in the experiments is shown in **Fig.**3.1. The laser chamber 1 had the length L_{ch} of 2.3 m along the optical axis. Totally reflected copper mirrors 2 and 3 were characterized by reflectance ~98.5% measured in spectral range of 2.5 - 3.5 μm. The spherical mirror 2 with radius of curvature of 5.0 m was fixed on the laser chamber (laser resonator length L_{las}= 2.5 m). The output window 4, plane parallel CaF_2 plate (diameter 160 mm, thickness 20 mm), was installed at an angle of 57^0 to the optical axis, that was not so far from Brewster angle (ϕ_B = 54.8^0; n = 1.42 for λ = 2-3 μm). An absorption of the plate measured in the range of 2.7 - 3.0 μm was 2% and in the range of 3.0 - 4.0 μm was less than 0.5% for a pass. A laser beam reflected from the output window was directed to the

photodetector. There was the diaphragm D with diameter of 47 mm in front of the mirror 3, that restricted the active volume of FO CO laser to the value of $V_{am}=L_{am}\,\pi d^2/4 \approx 2$ liter.

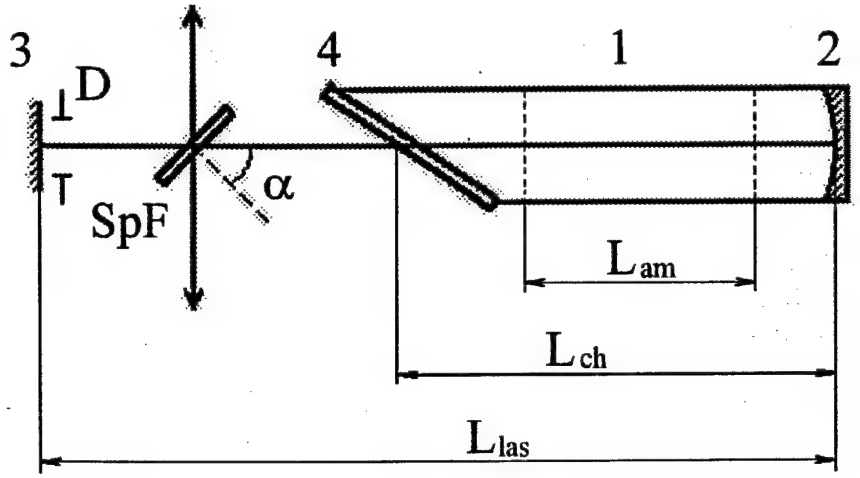

Fig.3.1. Schematic of FO CO laser resonator

1 - laser active medium with length L_{am}= 1.2 m;
2 - spherical totally reflected mirror;
3 - flat totally reflected mirror;
4 - CaF_2 window under Brewster's angle;
SpF - spectral filter;
D - diaphragm.
EBCD chamber length L_{ch} = 2.3 m.
Laser resonator length L_{las}= 2.5 m.

For a suppression of FB lasing the spectral filter SpF was installed between the laser mirror 3 and the output window 4. This optical filter was a thin plane parallel plate made of IR fused silica. It's dimensions were 100x100x1.9 mm^3. The spectral transmittance and Fresnel reflectance at normal incidence of radiation on the filter are demonstrated in **Fig.**3.2,a. Single-pass absorption of the filter was ~1.6% in the range of 2.7 - 3.3 μm. The radiation with wavelength longer than 5 μm was practically completely absorbed by the filter, that resulted in suppression of FB lasing. The laser output took place by Fresnel reflection from both sides of the filter SpF. The optical scheme used enabled us to change a resonator Q-factor by turning the filter relatively to the optical axis of the laser resonator (by changing the angle α). The calculated dependencies of double-pass total optical losses δ_{SpF} (1) (including absorption and reflection) for the filter, equivalent output coupling T_{eq} (2) and Q-factor (3) for the optical resonator on incidence angle α are represented in **Fig.**3.2.b (for the wavelength 3 μm). When calculating dependencies 2 and 3 the optical losses in the all optical elements of the laser resonator were taking into account. The equivalent output coupling T_{eq} (useful optical losses) was defined as a fraction of radiation power (relatively to the intracavity radiation power) going out of the optical resonator by Fresnel reflection on the both sides of the filter. Normally, the Q-factor of laser resonator is defined as a ratio of radiation energy inside the resonator to the total radiation energy losses for a period of oscillation: $Q_\lambda = 4\pi L_{las}/\lambda\Delta$, where λ is a wavelength of the radiation; $\Delta = \delta + T_{eq}$ is round-trip total optical loss ($\delta \approx 12\%$ - optical loss due to scattering from and absorption in totally reflected mirrors, output window and spectral filter). Bec... Q_λ

depends on λ for multiwavelength laser it would be much more convenient to use Q-factor attributed to a round-trip period of laser resonator instead of a period of electro-magnetic oscillation: $Q_{2L}=Q_\lambda \lambda/2L_{las}=2\pi/\Delta$ (see curve 3 in **Fig.**3.2.b).

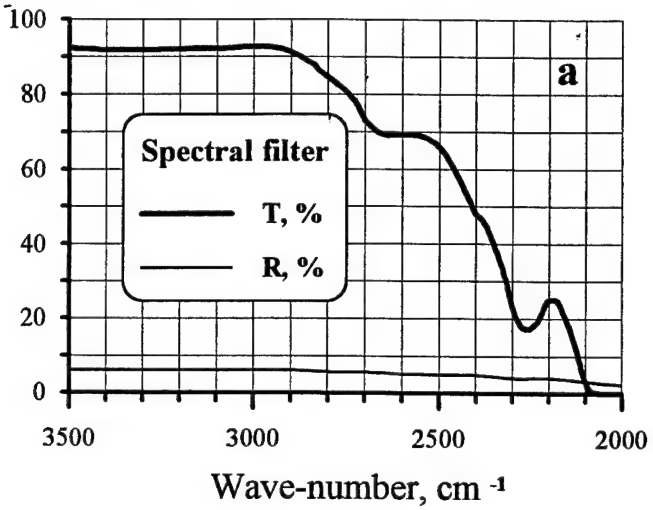

Fig.3.2a. Spectral characteristics of the filter SpF for FO CO laser: transmittance T and Fresnel's reflectance R at normal incidence.

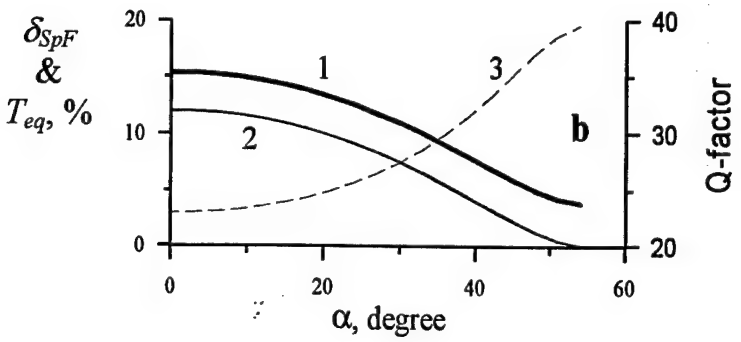

Fig.3.2b. Dependence of double-pass total optical losses δ_{SpF} of the filter SpF (1), equivalent output coupling T_{eq} (2) and Q-factor Q_{2L} (3) of the laser resonator (λ =3 μm) on angle α.

3.2 Characteristics of FO CO laser radiation

3.2.1. Spectral, temporal and spatial characteristics

In **Fig.**3.3 one can see a typical spectral distribution of output energy. It should be noted that the spectrum depended on experimental conditions (detailed research of the dependencies did not carried out in the experiments). FO lasing took place on V-V transitions from 13→11 up to 25→23 in the spectral range 2.7 - 3.3 μm. The upper limit of the spectral range was due to the spectral transmittance of the optical filter (see **Fig.**3.2.a). The lower border of the range was determined, as it would be demonstrated in the next chapter, by strong (up to 0.5 m^{-1}) absorption of FO CO laser radiation by intracavity atmospheric water vapor in the range of 2.5 - 2.7 μm. In special experiment we changed the length of the air column in the laser resonator from 0.2 up to 1.5 m, output energy being unchanged. The fact indicated that 0.2 m air column, being intracavity spectral selector, already formed a FO laser spectrum with λ>2.7 μm weakly absorbed by water vapors.

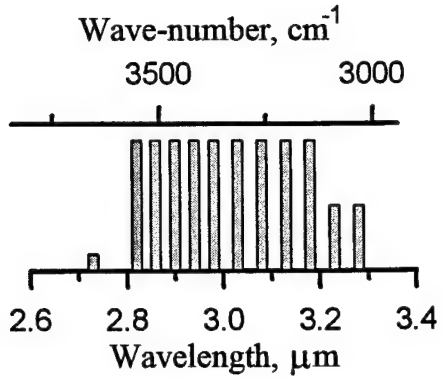

Fig.3.3. Spectrum of FO CO laser output.

Typical time-history of the EBCD current (which is very close to that of the input power or pumping pulse) and the laser output is shown in **Fig.**3.4. Pulse lengths for EBCD current t_{in}, for laser output t_{las} and time delay t_{delay} between the beginning of the current and the laser pulses were defined on 0.1 level relatively to their maximal values. Normally, the laser pulse length was hundreds of microseconds. Practically, in all the experiments the time delay was longer than the EBCD current pulse length ($t_{delay}>t_{in}$). It should be noted that the laser pre-pulse with an energy of more than the order of magnitude less than that of FO laser pulse was observed for time interval $t_{delay}> t > t_{in}$. This pulse was entirely absorbed when passing through plane parallel plate made of IR fused silica with a thickness of 5 mm and placed in front of a photodetector. One can assume that the pre-pulse is due to near threshold FB lasing on lower vibrational transitions with a wavelength not longer than 5 μm. The angular divergency of the FO laser was determined by laser resonator geometry and was not higher than 5 mrad.

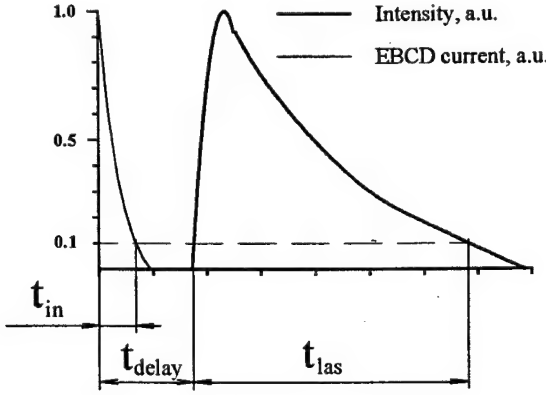

Fig.3.4. Time history of EBCD current pulse and that of FO CO laser pulse.
t_{in} - EBCD current pulse duration;
t_{delay} - time delay of laser output pulse;
t_{las} - laser output pulse duration.

3.2.2. Threshold lasing characteristics

A small signal gain (SSG) α_0 was experimentally measured by a technique of calibrated optical losses on the basis of following formula: $\exp(2\alpha_0 L_{am}) = [(1-\delta)(1-T_{eq})]^{-1}$. The additional plane parallel plate made of fused silica was placed into the laser resonator for changing the parameter δ by turning the plate relatively to the optical axis. The dependence of the output energy on the total optical losses $\delta+T_{eq}$ (where $T_{eq} = 6\%$) is demonstrated in **Fig.**3.5. FO lasing stopped at $\delta+T_{eq} \approx 30\%$, maximum of multiline spectrum SSG being $\alpha_0 \approx 0.14$ m^{-1}. The value of the SSG corresponded to a moment of time 200 μs for SIE (Q_{in}) of 270 J/l Amagat and 170 μs for 330 J/l Amagat.

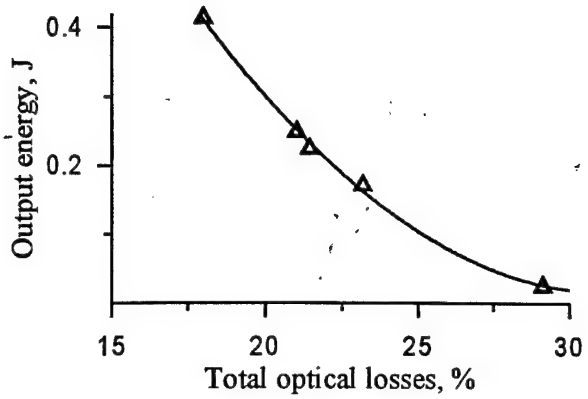

Fig.3.5. FO CO laser output energy versus total optical losses inside laser resonator. $CO:N_2 = 1:9$; $N = 0.3$ Amagat; aperture of laser output $d = 20$ mm in diameter and $V_{las}=0.4$ l; $Q_{in}= 300$ J/l Amagat; $t_{in}= 17$ μs.

3.2.3. Small signal gain

To determine the temporal behavior of SSG a time delay t_{delay}, i.e. a time interval needed for SSG to reach its threshold value (including laser pulse build-up time), was measured as a function of the total optical losses at the same experimental conditions ($CO:N_2=1:9$; $Q_{in}=300$ J/l Amagat; $N = 0.3$ Amagat). **Fig.**3.7 demonstrates the dependence of maximal multiline spectrum SSG on time, that was obtained by using data of **Fig.**3.6. The temporal behavior of the SSG can be approximated by logarithmic function $\alpha(t) = A\ ln(t/\tau)$, where $A \approx 0.067$ m^{-1}, and parameter $\tau=23$ μs is close to the $t_{in} = 17$ μs for the experimental condition. The empiric functional dependencies discribed the experimental ones, one of which is represented here, can be useful for a theoretical analysis in a future.

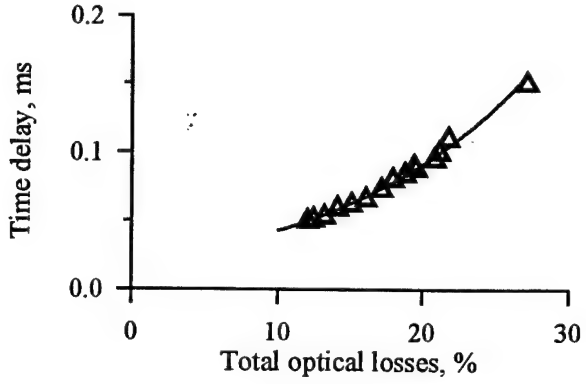

Fig.3.6. Time delay versus total optical losses inside FO CO laser resonator. $CO:N_2 = 1:9$; $N = 0.3$ Amagat; $Q_{in}= 300$ J/l Amagat; $t_{in}= 17$ μs.

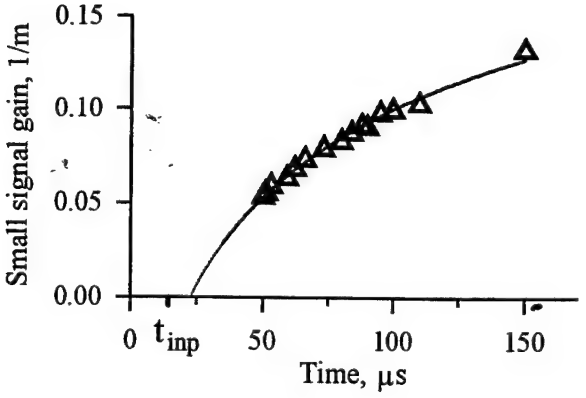

Fig.3.7. Time history of small signal gain was reconstruted due to the data of **Fig.**3.6.

3.3. Experimental parametric study of FO CO laser

3.3.1. Reference point of the parametric study

To compare experimental data and theoretical results, when studying FO CO laser, a reference point was chosen in a space of parameters varied in the experiments:

Table 3.1. Reference point of the parametric study

equivalent output coupling, T_{eq}	6%
laser mixture, CO : N_2 : He	1 : 9 : 0
gas density, N	0.3 Amagat
gas temperature, T	105 K
pumping pulse length, t_{in}	25 μs
SIE, Q_{in}	300 J/l Amagat

Only one parameter experimentally changed (if it is not specially pointed out) during the parametric study.

3.3.2. Equivalent output coupling of the laser resonator

The dependence of the specific output energy (SOE) on the SIE for the different output couplings T_{eq} and Q-factors of the laser resonator is demonstrated in **Fig.**3.8. The maximal SOE was observed at $Q_{2L} = 26$ and 27, that corresponded to the equivalent output coupling T_{eq} of 6.8 and 7.6%. **Fig.**3.9 demonstrates FO CO laser efficiency versus equivalent output coupling T_{eq} for the reference SIE of 300 J/l Amagat. The laser efficiency reached its maximum at a definite ratio of equivalent output coupling T_{eq} to the useless intracavity optical losses δ. For the experimental conditions the maximum lay in wide range of T_{eq} = 4-10%.

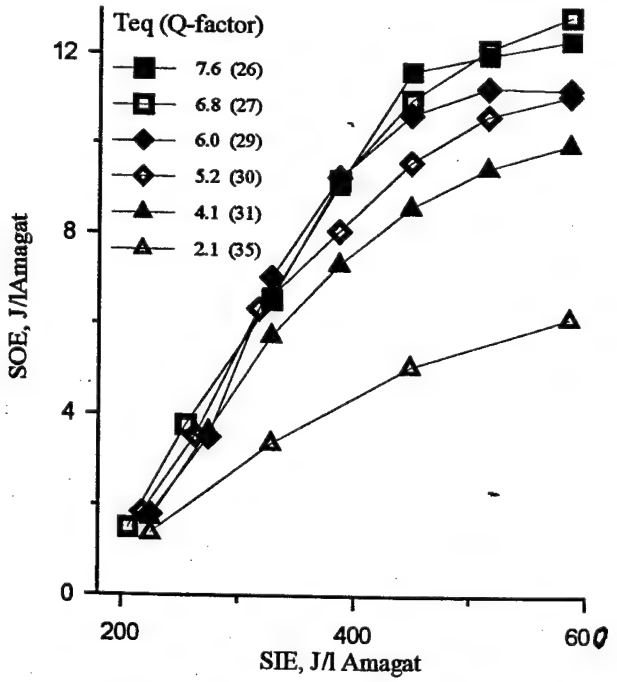

Fig.3.8. Specific FO CO laser output energy (SOE) versus specific EBCD input energy (SIE) for various equivalent output coupling T_{eq} (Q-factor Q_{2L}) of the laser resonator. N= 0.15 Amagat. Other parameters correspond to data from **Table** 3.1.

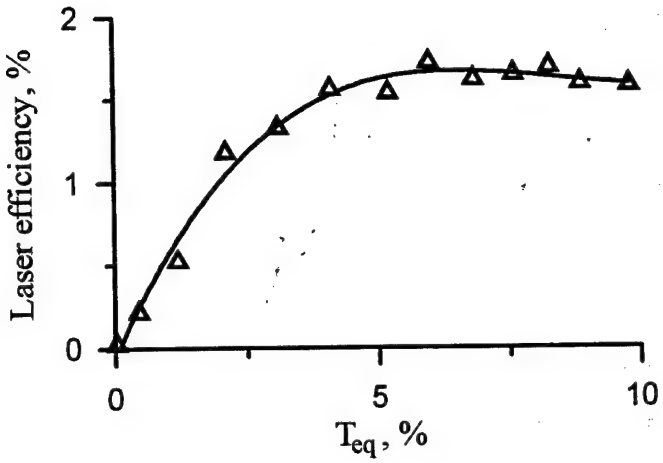

Fig.3.9 FO CO laser efficiency versus equivalent output coupling of laser resonator. Parameters correspond to data from **Table** 3.1.

Let's compare the results of the experiments with results for SSG obtained out of the threshold characteristics. To estimate the optimum value of output coupling T_{eq}^{opt}, when maximal laser efficiency is reached, we used the simplified formula (Ichshenko et al., 1968) $T_{eq}^{opt} = (2\alpha_0 L_{am}\delta)^{0.5} - \delta$. By substituting the parameters $2\alpha_0 L_{am} = 30\%$ and $\delta = 12\%$ into the formula we obtained $T_{eq}^{opt} = 7\%$, that corresponds to the center point of the interval $T_{eq} = 4\text{-}10\%$ obtained in direct experiments on the output efficiency as a function of the equivalent output coupling (**Fig.**3.9). To characterize the dependence $T_{eq}^{opt} = T_{eq}^{opt}(\delta)$ it is useful to introduce the parameter $x=(\delta/2\alpha_0 L_{am})^{0.5}$, which describes the useless optical losses as compared to an amplification factor $2\alpha_0 L_{am}$. Thus $T_{eq}^{opt} = 2\alpha_0 L_{am}(x\text{-}x^2)$, and maximal laser efficiency $\eta \sim (1\text{-}x)^2$. For the experimental conditions (**Table** 3.1) $x \approx 0.63$. Let's designate the laser efficiency as η_0 for the conditions. When the useless optical losses decrease down to $\delta = 3\%$ ($x = 0.31$), the optimum output coupling decreases down to $T_{eq}^{opt} = 0.42\alpha_0 L_{am} = 6.3\%$ and $\eta = 3.5\eta_0$, i.e. the laser efficiency three times as much as that of previous case. The maximal $T_{eq}^{opt} = \alpha_0 L_{am}/2 = 7.5\%$ takes place at $x = 0.5$ and $\delta = \alpha_0 L_{am}/2 = 7.5\%$. The rough analysis fulfilled demonstrated that at the same amplification factor maximal laser efficiency could be increased three times only due to four times decrease of useless optical losses. The optimum output coupling T_{eq}^{opt} for our experimental conditions, i.e. for given optical elements of the laser resonator, lies within the range of 6-7.5%.

3.3.3. Specific input energy

In **Fig.**3.10 one can see a dependence of SOE on SIE for two laser mixtures $CO:N_2:He = 1:9:10$ and 1:9:0. The threshold SIE was ~100 J/l Amagat for the helium-containing gas mixture 1:9:10 and ~150 J/l Amagat for the helium-free gas mixture 1:9:0. When increasing SIE, the SOE increased approximated linearly. The maximal SOE for the gas mixture 1:9:10 was twice as much as that of two-component gas mixture 1:9 (the detailed discussion about an influence of gas mixture composition on laser characteristics see below in 3.3.7).

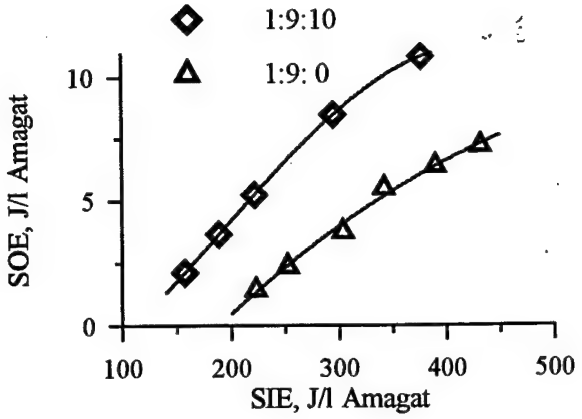

Fig.3.10. Specific FO CO laser output energy (SOE) versus specific input energy (SIE) for different gas mixtures $CO:N_2:He = 1:9:10$ and 1:9:0. Other parameters correspond to data from **Table** 3.1.

Figs.3.11 and 3.12 give a more detailed information about the energetic characteristics (SOE and laser efficiency) of the laser using 1:9:10 gas mixture for different capacitances of the capacitor bank (the analysis of the influence of the EBCD parameters on the laser characteristics see in 3.3.5). One can see from **Fig.**3.11 that at SIE higher than 300-350 J/l Amagat corresponding to the maximal laser efficiency of 3.0% (**Fig.**3.12) the dependence of SOE on SIE is saturated. The reason for the effect observed could be a gas temperature rise due to a heating of the laser mixture - the effect well known for CO_2 lasers. The other confirmation of the explanation could be the sharp decrease of the laser pulse length when SIE increases higher than ~350 J/l Amagat (**Fig.**3.13) for given experimental conditions (see also 3.3.6 and 3.3.7). In **Fig.**3.13 one can see the laser pulse duration and time delay versus SIE for the laser mixture 1:9:10. When the SIE increased from the threshold value up to 500 J/l Amagat the time delay decreased. The laser pulse length also increased up to 1.2 ms, being approximately the same for SIE of 200-300 J/l Amagat, and decreased at further increase of the SIE.

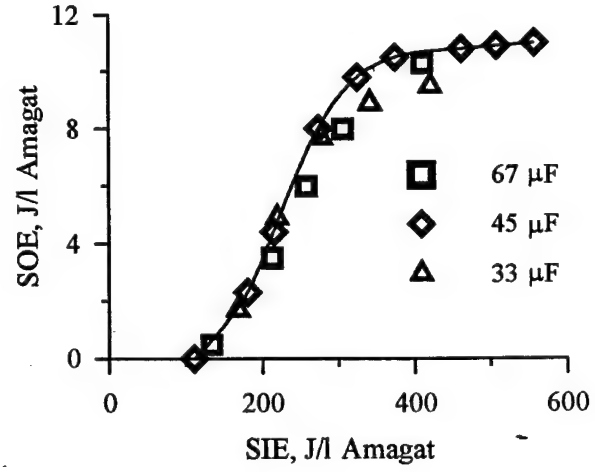

Fig.3.11. Specific output energy (SOE) versus specific input energy (SIE) $CO:N_2:He=1:9:10$. Other parameters from **Table**-3.1.

For given experimental conditions (**Fig.**3.10-3.13, laser mixture $CO:N_2:He = 1:9:10$) the maximum of the laser efficiency 3.0% corresponded to SIE ≈320 J/l Amagat. For the gas mixture $CO:N_2 = 1:9$ the laser efficiency reached its maximum 1.7% at SIE ≈400 J/l Amagat.

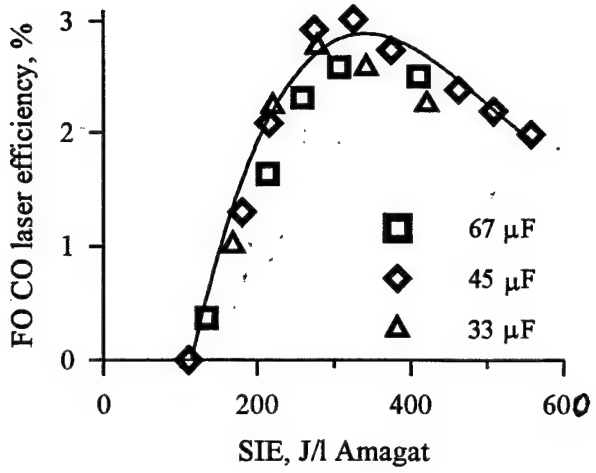

Fig.3.12. FO CO laser efficiency versus specific input energy (SIE) for data of **Fig.**3.11.

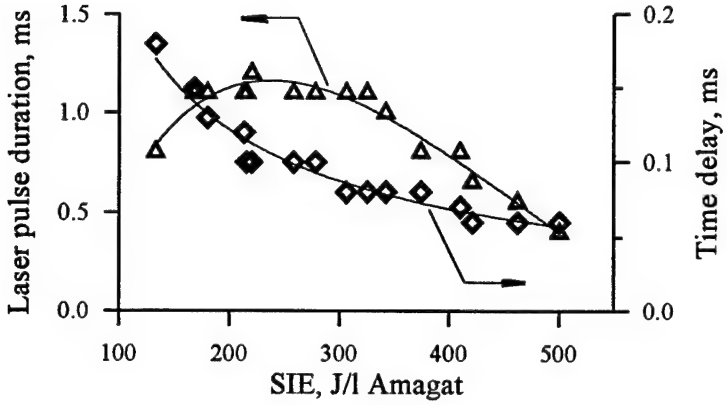

Fig.3.13. Laser pulse duration and time delay versus specific input energy (SIE) for data of **Fig.**3.11.

3.3.4. Gas temperature

The dependence of the SOE on the gas temperature for two different values of the SIE 270 and 330 J/l Amagat one can see in **Fig.**3.14. During the experiment the gas temperature decreased from 300 K down to 104 K. For the SIE ≈ 330 J/l Amagat FO CO lasing started at T_{th}≈170 K. For the SIE equaled 270 J/l Amagat T_{th}≈160 K. The decrease of the gas temperature led to the increase of the laser efficiency as in the case of the FB CO laser.

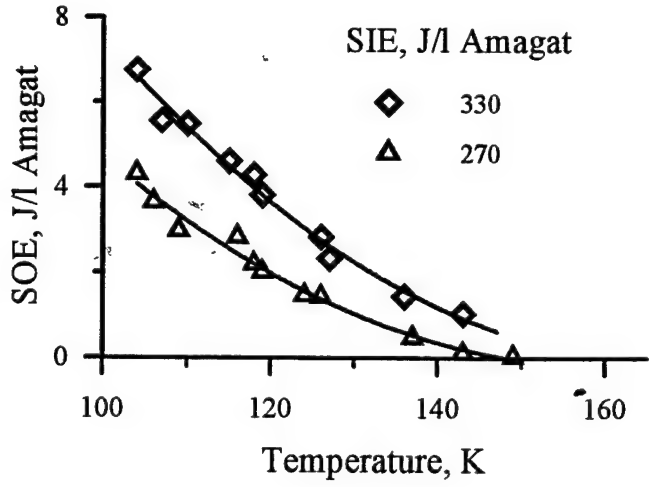

Fig.3.14. Specific FO CO laser output energy (SOE) versus gas temperature for different specific input energy (270 and 330 J/l Amagat). Other parameters correspond to data from **Table** 3.1.

Computer analysis of the experimental data demonstrated that the dependence of the SOE on the gas temperature could be represented by the expression $Q_{out}(T) \sim exp(-T/T_0)$, where $T_0 \approx 20$ K, or more exactly by a second degree polynomial $Q_{out}(T) = W(T/T_1 - 1)^2$, where $T_1 \approx T_{th}$, $W \approx 35$ J/l Amagat for Q_{in}=270 J/l Amagat and $W \approx 47$ J/l Amagat for Q_{in}=330 J/l Amagat.

3.3.5. Temporal characteristics of EBCD and FO CO laser

During the EBCD current pulse the EBCD voltage changed in accordance with a dependence $U(t) = U_0(1-exp(-t/RC))$, where $R(t) = 1/G(t)$ - electrical resistance of a laser mixture, the electrical conductivity of which $G(t)$ is due to gas ionization by e-beam current $j(t)$. The temperature of the secondary electrons in the electric discharge plasma is determined by the reduced electric field strength E/N. Therefore the change of the electric field strength during the EBCD influences upon the effectiveness of the excitation of CO molecule vibrational levels and gas heating. For changing a temporal behavior of the discharge voltage pulse we varied capacitance of the capacitor bank. **Fig.**3.11 and 3.12 demonstrate the energetic characteristics (SOE and laser efficiency) of the laser versus SIE for laser mixture CO:N_2:He=1:9:10 and for different capacitances C=33; 45 and 67 μF, i.e. for different initial/end discharge voltage ratio 3.3, 2.7, and 2.2 accordingly. It should be pointed out, that usage of capacitance of 80 μF led to the higher end discharge voltage and, as a result, to the electrical breakdown after the EBCD current pulse, laser pulse distortion and a decrease of SOE. To get even very low SIE of~200 J/l Amagat for lower capacity of 12 μF one should use very high initial voltage that also led to the electrical breakdown but during the pumping pulse. From **Fig.**3.11 and 3.12 one can conclude that there is no noticeable influence of temporal behavior of the EBCD voltage on the laser characteristics when the capacitance changed between 30 and 70 μF. However, one should take into consideration that initial discharge voltage changed as $C^{-0.5}$ when changing the capacitor capacitance C, i.e. it changed 1.5 times at the same SIE. Therefore at the moment we cannot definitely make a conclusion about the influence of the pumping pulse shape on the laser characteristics.

In the experiments we also researched the effect of the pumping pulse length on the energetic characteristics of the laser. The pumping pulse length t_{in} varied within 25-1500 μs interval by changing the heating of the thermoionic cathode and, hence, by changing e-beam current density and EBCD resistance $R(t)$. The dependence of the SOE on the pumping pulse length for the gas mixture CO:N_2=1:9 and the SIE of ~300 J/L Amagat is shown in **Fig.**3.15. One can see a sharp decrease of the SOE with an increase of the pumping pulse duration. At t_{in}>250 μs the output energy decreased more than two orders of magnitude. The curve in the **Fig.**3.15 can be described by the expression $Q_{out}(t_{in}) = B(t_{in}/\tau_2 - 1)^2$, where $t_{in} < \tau_2 \approx 270$ μs, $B \approx 5.3$ J/L Amagat.

Time delay t_{delay} of laser pulse versus the pumping pulse length is shown in **Fig.**3.16. An increase of t_{in} from 25 μs up to 300 μs led to approximately linear growth of $t_{delay} = \beta_0 + \beta_1 t_{in}$, where $\beta_0 \approx 50$ μs, $\beta_1 \approx 2$, i.e. t_{delay} was twice as much as pumping pulse length.

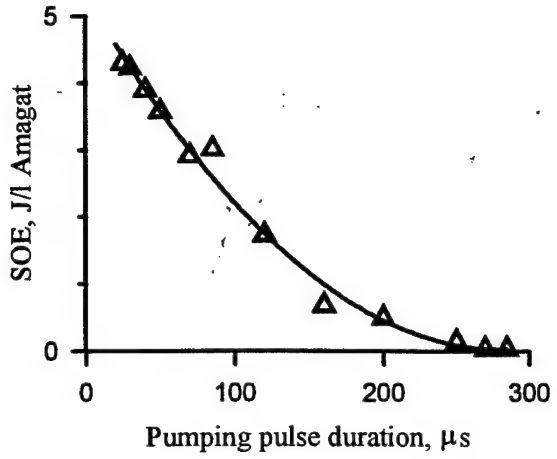

Fig.3.15. Specific FO CO laser output energy (SOE) versus input pulse duration. Parameters correspond to data from **Table** 3.1.

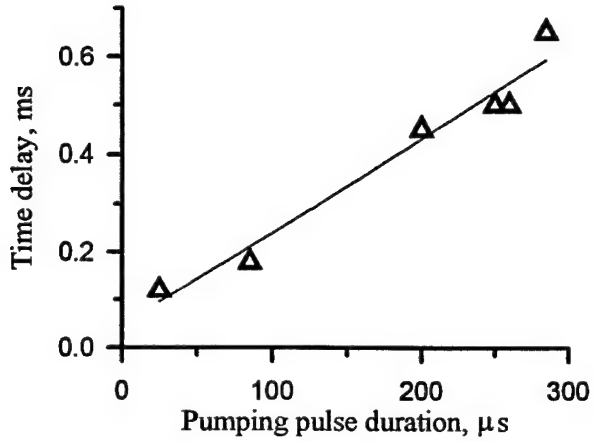

Fig.3.16. Time delay versus pumping pulse duration t_{in}. Parameters correspond to data of **Fig.**3.15.

Fig.3.17 demonstrates the dependence of the SOE on the SIE for the different pumping pulse length t_{in}= 25; 85 and 160 μs. It should be pointed out that the threshold SIE increased twice from 100 up to 200 J/l Amagat when t_{in} increased from 25 up to 160 μs. It is necessary also to mark that at the same parameter E/N = 3.5 kV/cm Amagat the increase of pumping pulse from 25 up to 280 μs led to the SIE growth from 260 up to 310 J/l Amagat, initial/end discharge voltage ratio increasing by 10%.

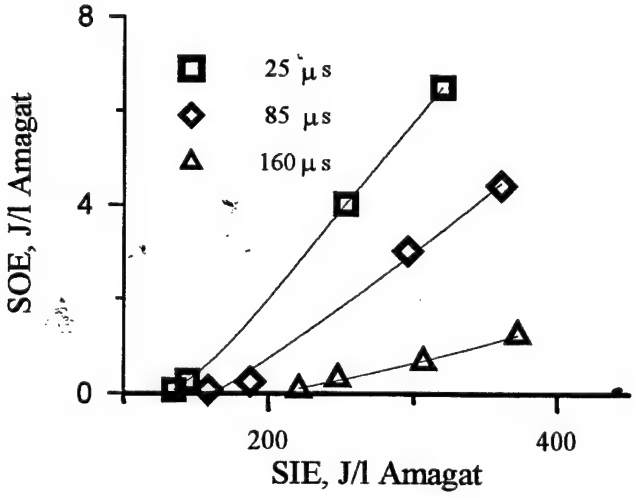

Fig.3.17. Specific FO CO laser output energy (SOE) versus specific input energy (SIE) for different pumping pulse duration.
Parameters correspond to data of **Fig.**3.15.

The effect of pumping pulse length on temporal behavior of the FO laser pulse was also studied experimentally (**Fig.**3.18). The initial EBCD current was the same for the different cases represented in the **Fig.**3.18. The interruption of the EBCD current was effected by e-beam current interruption by an electrical crowbar. One can see from **Fig.**3.18a that the long pumping pulse of 1200 μs duration led to a very weak lasing ($t_{delay} \approx 600$ μs; $t_{las} \approx 200$ μs). The output energy was of two orders of magnitude less than for $t_{in} \leq 100$ μs. At shorter pumping pulse ($t_{in} \approx 800$ μs) one can see in **Fig.**3.18b a sharp increase of the laser pulse just after the pumping pulse is over, the output energy increasing 5 times. At further pumping pulse shortening the output energy is 20 times (**Fig.**3.18c) and 200 times (**Fig.**3.18d) higher as compared to data of **Fig.**3.18a. When shortening the pumping pulse the time delay is diminished and output pulse length increases. Thus despite the fact that the SIE decreased the the SOE increased for shorter pumping pulse. The effect observed could be explained by overheating of the laser mixture for longer pumping pulse, but for the sharp increase of laser intensity had taken place in **Fig.**3.18b just after the pumping pulse. The same effect was observed for FB CO laser (Basov et al, 1980c) and can be explained by superelastic electron collisions with CO molecules. The experimental results indicate that for the experimental conditions it is much better to use shorter pulses for FO CO laser pumping.

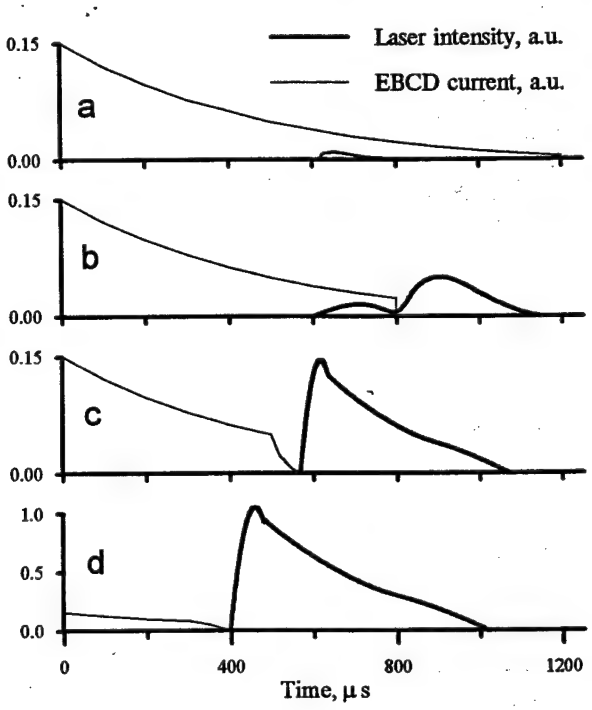

Fig.3.18. Time history of laser output for different pumping pulse duration.
Parameters correspond to data from **Table** 3.1.

3.3.6. Gas density

Gas density for the reference laser mixture $CO:N_2$ = 1:9 varied from 0.5 down to 0.15 Amagat. **Fig.**3.19 demonstrates the SOE versus the SIE for different gas densities. The maximal SOE of 10-12 J/l Amagat and maximal laser efficiency ~2% was observed for $N = 0.15$ Amagat. The increase of gas density up to $N = 0.5$ Amagat led to a practically linear decrease of the laser pulse duration t_{las} from

1000 μs down to 300 μs (**Fig.**3.21). The dependence can be empirically described as $t_{las}(N) = -2.0\,N + 1.3$ (ms).

The experiments with gas density lower than 0.15 Amagat were carried out on another EBCD laser installation with electric discharge volume ~2 liter and active length L_{am}= 1.5 m. Because of non-optimal experimental conditions (the high gas temperature T = 130-150 K; the long input power pulse duration $t_{in} \approx$ 50 μs; both totally reflected mirrors were placed outside laser chamber; two CaF_2 output windows on the chamber were used) the dependence of the SOE on the SIE for different gas densities lower than 0.15 Amagat are presented in arbitrary units (**Fig.**3.20). One can see that a decrease of density from 0.1 Amagat down to 0.02 Amagat led to a decrease of the SOE and laser efficiency. When changing the density between 0.15 and 0.04 Amagat, the threshold SIE practically did not change and was equal ~200 J/l Amagat.

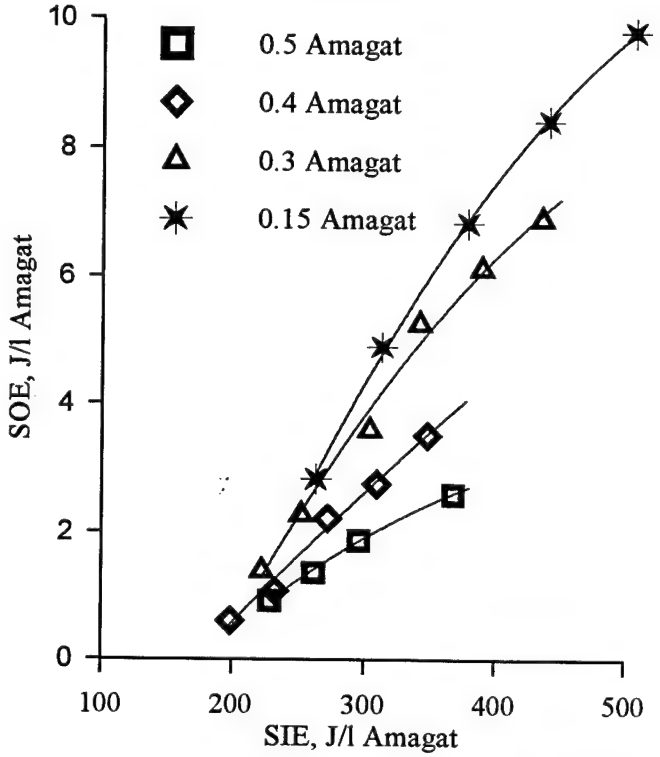

Fig.3.19. Specific FO CO laser output energy (SOE) versus specific input energy (SIE) for various gas density N = 0.15 - 0.5 Amagat. Other parameters correspond to data from **Table**3.1.

Fig.3.22 demonstrates the dependence of t_{las} and t_{delay} on gas density N at the SIE ≈800 J/l Amagat (such a high SIE was easily obtained at lower gas densities). The decrease of N from 0.15 down to 0.02 Amagat resulted in an increase of t_{las} from 900 up to 3000 μs, t_{delay} increasing from 80 up to 500 μs. The empirical dependence can be described as $t_{las}(N) = \tau_{las} N^{-0.58}$ and $t_{delay}(N) = \tau_{delay} N^{-0.82}$, where $\tau_{las} \approx$ 320 μs and $\tau_{delay} \approx$ 15 μs. At gas density 0.22 Amagat a linearized formula for t_{las} can be expressed as $t_{las}(N) = -2\,N + 1.2$ (ms) and is in a good agreement with dependency shown in **Fig.**3.21 at N = 0.15-0.5 Amagat, although at the different SIE. The increase of time delay with the decrease of gas density is connected with time needed for vibrational excitation to get to the vibrational levels of CO molecule taking part in lasing process.

Optimum SIE for the laser mixture $CO:N_2 = 1:9$ at gas density less than 0.1 Amagat practically did not depend on gas density and was ~1000 J/l Amagat. Some decrease of the SOE at the higher SIE was due to overheating of laser mixture.

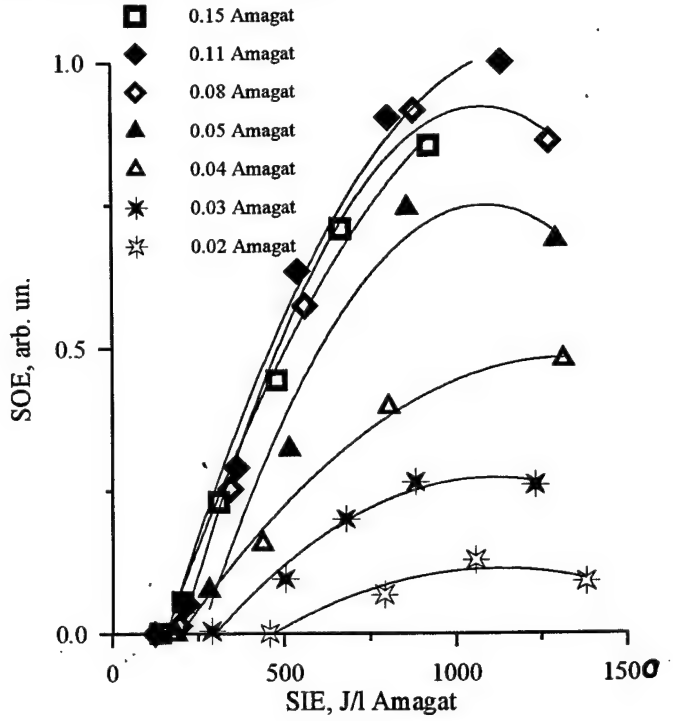

Fig.3.20. Specific FO CO laser output energy (SOE) versus specific input energy (SIE) for various gas density $N = 0.02 - 0.15$ Amagat. Experiment was carried out with another laser installation.

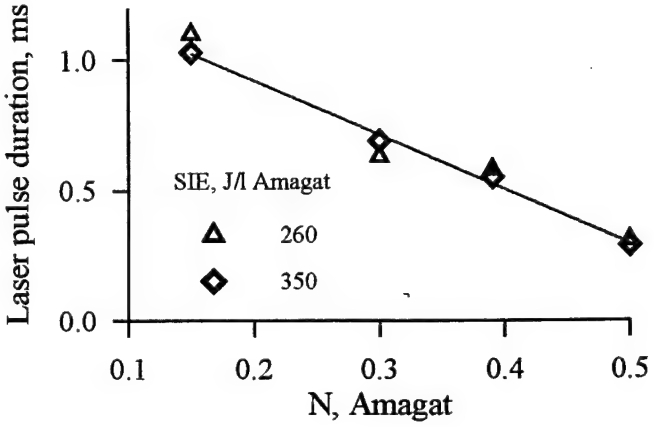

Fig.3.21. FO CO laser pulse duration versus gas density for SIE 260 and 360 J/l Amagat. Other parameters correspond to data of **Fig.**3.19.

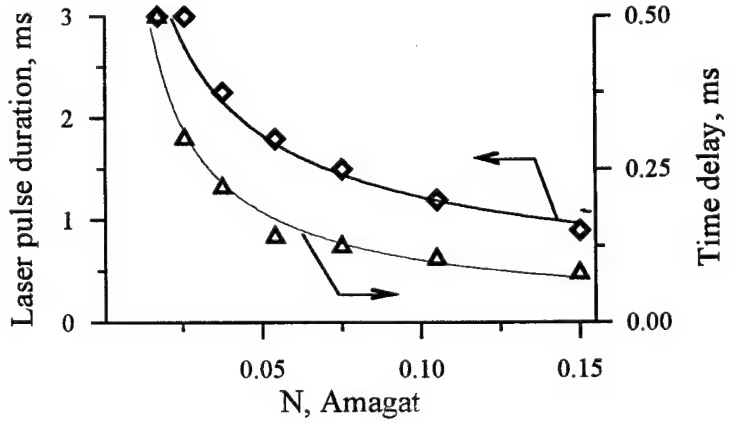

Fig.3.22. FO CO laser pulse duration and time delay versus gas density at SIE 800 J/l Amagat. Other parameters correspond to data of **Fig.**3.20.

When analysing the experimental data in **Figs.**3.19 and 3.20 there were obtained the dependencies of the SOE on gas density at the fixed value of the SIE 300 J/l Amagat (**Fig.**3.23) and 300, 500 and 700 J/l Amagat (**Fig.**3.24). An increase of gas density from 0.15 up to 0.5 Amagat resulted in approximately linear decrease of the SOE (**Fig.**3.23). When decreasing gas density from 0.1 Amagat down to 0.02 Amagat, laser output practically decreased to zero, i.e. at gas density 0.02 Amagat there was a lasing threshold independently of the SIE. The reason for the effect observed seems to be a rise of role of Doppler spectral broadening, which is comparable with pressure broadening just at 0.02 Amagat, and, hence, a decrease of the SSG with a decrease of gas density. A comparison of dependencies of **Figs.**3.23 and 3.24 enables us to make a conclusion that for the laser mixture $CO:N_2$ = 1:9 at given experimental conditions the optimum (from the point of view of the SOE in J/l Amagat units) gas density is ~0.1 Amagat. The SIE can be increased up to 1000 J/l Amagat. **Fig.**3.25 combining **Figs.**3.23 and 3.24 demonstrates, that although N=0.1 Amagat laser is characterized by higher laser efficiency, N=0.4 Amagat is more suitable for having higher laser output from given volume unit at the constant SIE (300 J/l Amagat). The maximum SOE was 2 J/l at the SIE 450 J/l Amagat and N=0.3 Amagat.

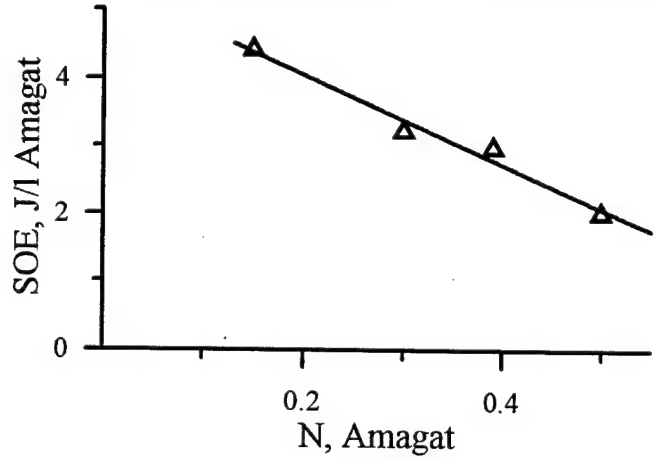

Fig.3.23. Specific FO CO laser output energy (SOE) versus gas density N in Amagat. Other parameters correspond to data of **Fig.**3.19 with SIE 300 J/l Amagat.

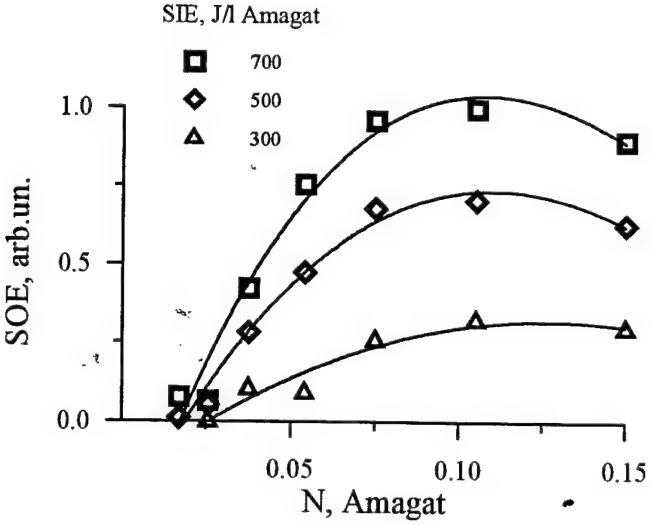

Fig.3.24. Specific FO CO laser output energy (SOE) versus gas density for various specific input energy (SIE 300, 500 and 700 J/l Amagat). Other parameters correspond to data of **Fig.**3.20.

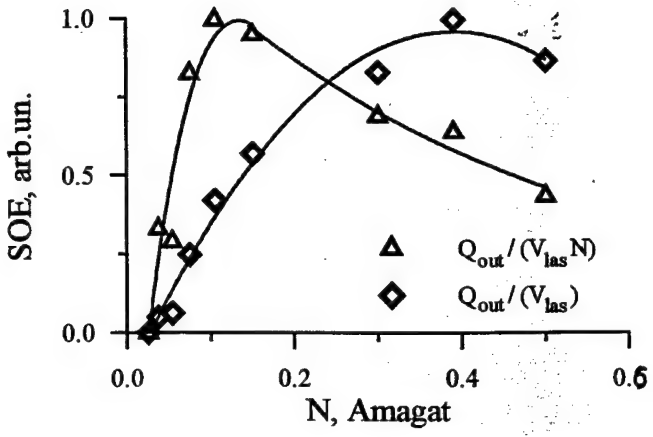

Fig.3.25. SOE in ***J/l Amagat*** $Q_{out}/(V_{las}N)$ and ***J/l*** units $Q_{out}/(V_{las})$ versus laser mixture density for data of **Figs.**3.23 and 3.24.

3.3.7. Laser mixture composition

It was already demonstrated (**Fig.**3.10) that the composition of laser mixture extremely effected on energetic characteristics of the FO CO laser. The dependence of the SOE on nitrogen content in two component laser mixture $CO:N_2$ is shown in the **Fig.**3.26 (Q_{in}=300 J/l Amagat).When increasing nitrogen content from 60% up to 90%, the SOE increased approximately linearly more than 3 times. The maximal SOE was observed at 90% nitrogen content (gas mixture 1:9). **Fig.** 3.27 demonstrates time delay t_{delay} versus nitrogen content for two different SIE 250 and 320 J/l Amagat. The time delay practically did not change, when nitrogen content varied between 60 and 90%. The further rise of N_2 percentage resulted in a sharp of t_{delay} from ~0.1 up to 0.3 ms and a decrease of the SOE (**Fig.**3.26). The SOE for the laser mixture $CO:N_2$ = 1:35 was a half as much as that of the gas mixture 1:9.

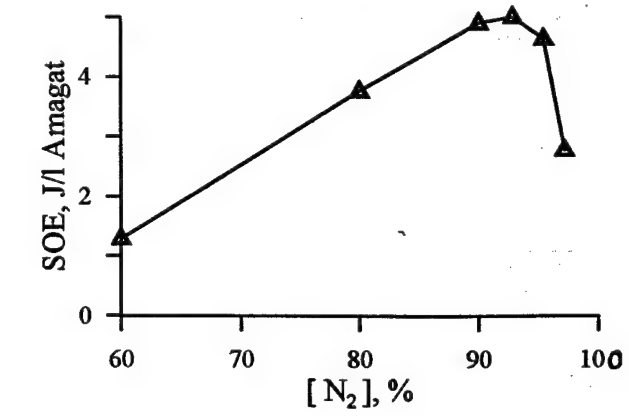

Fig.3.26. Specific FO CO laser output energy (SOE) versus N_2 content in gas mixture $CO:N_2$. Other parameters correspond to data from **Table** 3.1.

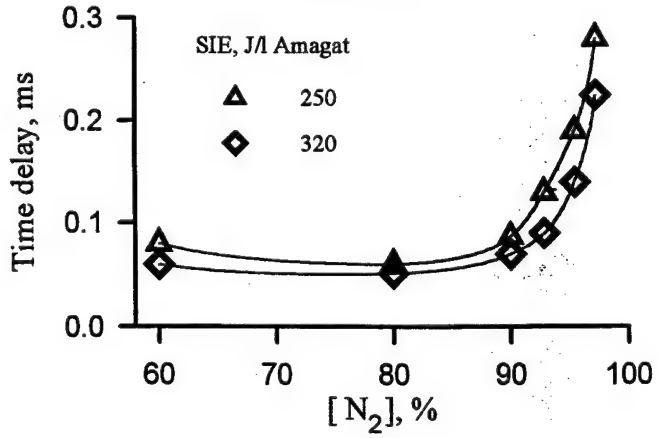

Fig.3.27. Time delay versus N_2 content in gas mixture $CO:N_2$ for SIE 250 and 320 J/l Amagat. Other parameters correspond to data of **Fig.**3.26.

The dependence of the SOE on helium content (**Fig.**3.28) for the laser mixture CO:N_2:He = 1:9:x is more smooth as compared to that of **Fig.**3.26 (N = 0.15 Amagat; Q_{in}= 300 J/l Amagat). When He content was up to 50%, the SOE increased 1.5 times, its maximum value being for the laser mixture CO:N_2:He = 1:9:10. **Fig.**3.29 demonstrates the time delay t_{delay} versus helium content for three different SIE.

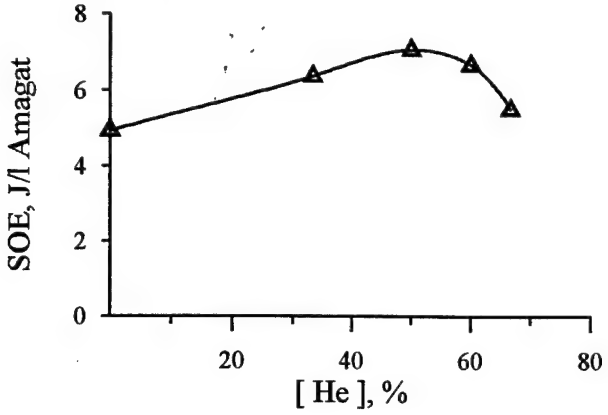

Fig.3.28. Specific FO CO laser output energy (SOE) versus He content *100 x /(1+9+x)* in gas mixture CO:N_2:He=1:9:*x*. N = 0.15 Amagat. Other parameters correspond to data from **Table** 3.1.

The dependencies of the SOE on the SIE for different helium content are shown in **Fig.**3.30 (N = 0.15 Amagat). The highest threshold SIE was observed for helium-free mixture. At SIE > 300 J/l Amagat SOE was practically the same one for laser mixtures with 0%; 33% and 50% helium content. At higher helium percentage the maximal value of SOE decreased. At 83% helium content an electrical breakdown took place at SIE > 250 J/l Amagat.

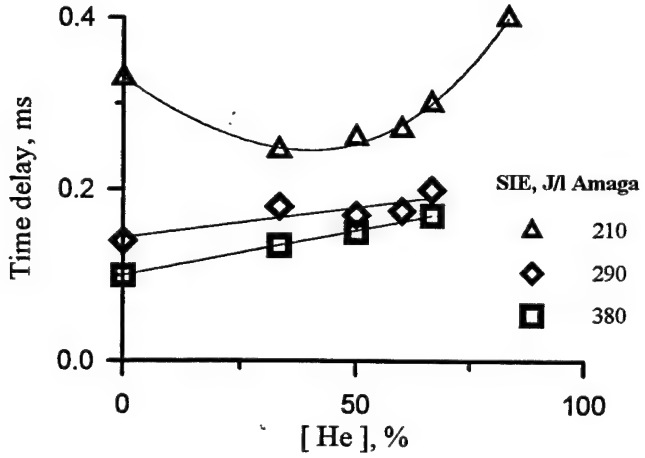

Fig.3.29. Time delay versus He content *100 x /(1+9+x)* in gas mixture CO:N_2:He = 1:9:*x* for SIE 210, 290 and 380 J/l Amagat. Other parameters correspond to data of **Fig.**3.28.

Figs.3.31 - 3.33 represent results of the experiment in which the content of molecular components (CO:N_2 = 1:9) was kept constant, only helium density being increased. Thus the number of vibrationally excited molecules was unchanged, laser mixture density being varied only by changing buffer gas (He) density. The maximal SOE was approximately the same for helium-free mixture and mixture with 33% helium content. Although at the same SIE the SOE for helium-free mixture was less than for helium containing ones. It should be noted out that the maximal specific energy output in J/l units was higher for the laser mixture with 50% helium content and reached ~3 J/l. The influence of helium can be easily seen in **Fig.**3.33 where the dependence of the SOE reduced to a partial density of molecular gases CO and N_2

($CO+N_2$) on the SIE (at the same units) is shown. The increase of He content led to the decrease of the SOE in J/l Amagat ($CO+N_2$) units at the same value of the SIE, that can be connected with a higher V-T relaxation rate of molecular gases at higher He content.

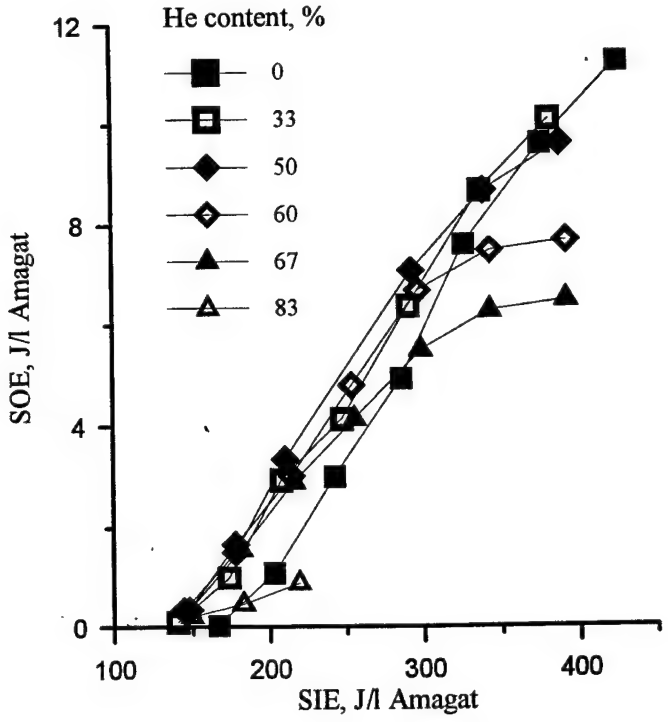

Fig.3.30. Specific output FO CO laser energy (SOE) versus specific input energy (SIE) for various He content $100\,x/(1+9+x)$ in gas mixture $CO:N_2:He = 1:9:x$. N= 0.15 Amagat. Other parameters correspond to data from **Table** 3.1.

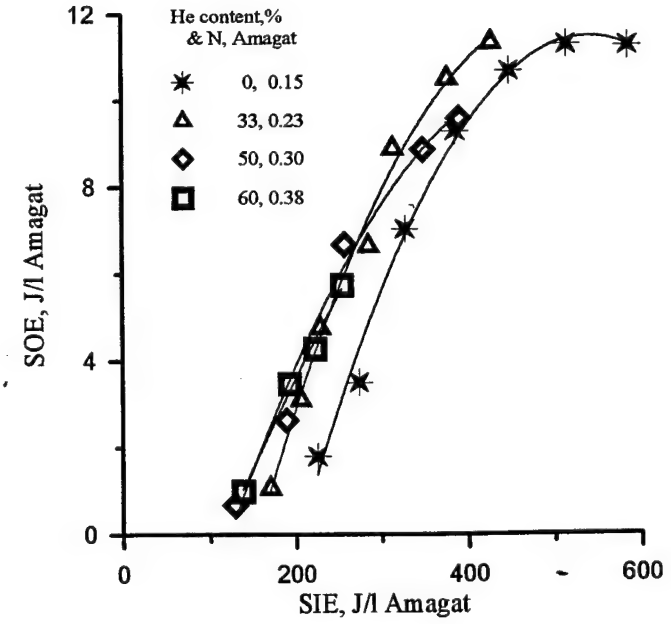

Fig.3.31. Specific laser output energy versus specific input energy for different He content $100\,x/(1+9+x)$ in gas mixture $CO:N_2:He=1:9:x$ with constant partial density of $CO+N_2$ molecules. Other parameters correspond to data from **Table** 3.1.

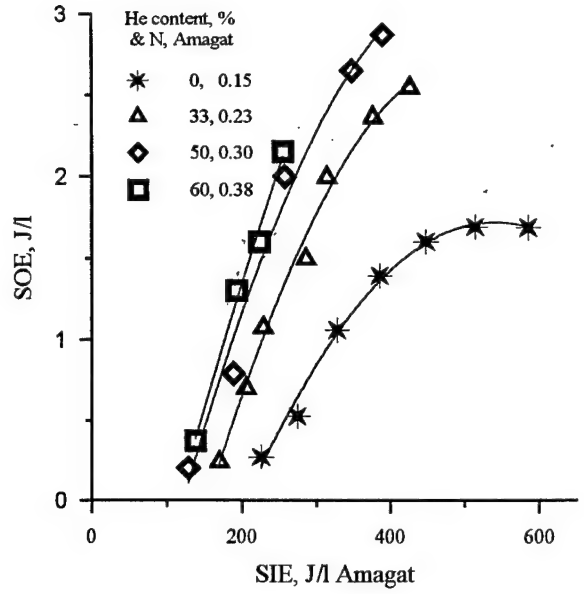

Fig.3.32. Specific laser output energy in ***J/l*** units versus specific input energy in ***J/l Amagat*** units for different He content $100\,x/(1+9+x)$ in gas mixture $CO{:}N_2{:}He=1{:}9{:}x$ with constant partial density of $CO+N_2$ molecules. Experimental data presented in this **Fig.** are the same ones as in **Fig.**3.31.

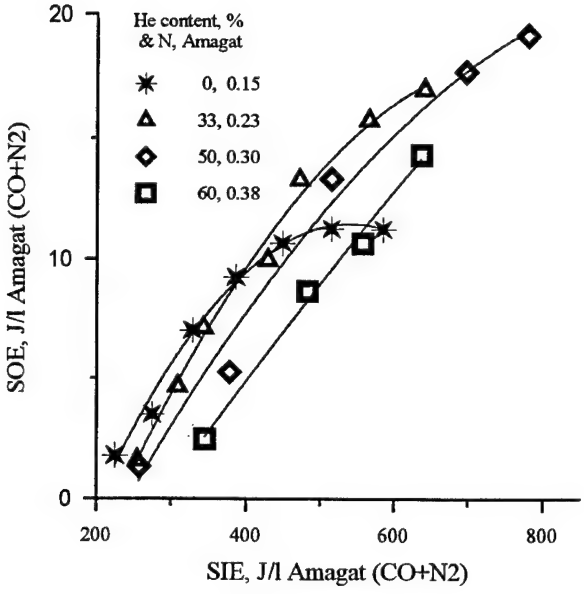

Fig.3.33. Specific laser output energy versus specific input energy reduced to $CO+N_2$ partial density. Experimental data presented in this **Fig.** are the same ones as in **Fig.**3.31.

3.4. Discussion of the experimental results and conclusions

The experimental parametric study was aimed at the research of an influence of different parameters varied in the experiments on energetic characteristics of FO CO laser and, first of all, on output energy and laser efficiency. The following conclusions can be formulated:

1. FO CO lasing was obtained, FB CO lasing being suppressed by specially developed spectral filter. The time-history of the SSG was determined. The maximum SSG at reference parameters (**Table** 3.1) was ~0.14 m^{-1}. The optimal equivalent output coupling T_{eq} at given SSG, active length and optical losses lies at the range of 4-10%.

2. The most optimum laser mixture under the experimental conditions is $CO{:}N_2{:}He$ = 1:9:10, maximum laser efficiency being 3% (N=0.3 Amagat, SIE is 350 J/l Amagat). Despite high useless optical losses (~12% per round-trip) the maximum SOE is 11 J/l Amagat and 3.3 J/l (N=0.3 Amagat, SIE is

500 J/l Amagat). The more important factor is carbon monoxide/nitrogen ratio as compared to helium percentage.

3. The optimum helium-free laser mixture is $CO:N_2$ =1:9. For the gas mixture the laser efficiency is 1.7% at N=0.3 Amagat, being 2.4% at N=0.15 Amagat. From the point of view of the maximum laser efficiency and SOE in J/l Amagat units, optimum gas density is 0.1 Amagat. The maximum SOE measured in the experiments reaches 12 J/l Amagat (N=0.15 Amagat, SIE 600 J/l Amagat). From the point of view of the maximum SOE in J/l units, that is very important for geometric characteristics of FO CO laser, the optimum gas density for the same mixture is 0.4 Amagat (SIE is 300 J/l Amagat), SOE being 1.2 J/l. The maximum SOE measured in the experiments reaches 2 J/l (N=0.3 Amagat, SIE 450 J/l Amagat).

4. The optimum SIE (from the point of view of maximum SOE) depends both on gas density and laser mixture composition. At lower densities (<0.1 Amagat) the optimum SIE for two-component mixture $CO:N_2$ = 1:9 was 1000 J/l Amagat. At N = 0.5 Amagat the maximum SIE of 400 J/l Amagat was restricted by electric discharge breakdown. When increasing gas density higher than 0.1 Amagat, the optimum SIE decreases, being close to the maximal SIE determined by the electrical breakdown. When using helium containing mixture, the optimum SIE decreases down to 250-350 J/l Amagat.

5. The usage of the special laser mirror (output coupler) with output coupling 4-10% (R_{out}= 90 - 96%) in 2.5 - 4.2 μm spectral region with low reflectance (<0.5%) in 4.9 - 6.0 μm band installed on laser chamber directly will enable us to eliminate useless optical losses connected with spectral filter, CaF_2 output window and water vapor absorption, to widen the laser spectrum and hence, to increase a laser output. When decreasing useless optical losses from 12% per round-trip in the experiment down to 3% in future, the laser efficiency expected could be 10%.

6. The energetic characteristics of the laser are strongly depend on gas temperature, the dependence of SOE on gas temperature within the range of 160 K - 100 K being practically square one.

7. Taking into consideration the strong dependence of the SOE on gas temperature one can conclude that a part of electric discharge energy going into the heating should be diminished. Therefore the time-history of discharge voltage pulse was not optimum one, because of 2-3 times decrease of the discharge voltage to the end of the voltage pulse. A rectangular shape of the voltage pulse would be more preferable. Although the experiments with different capacities did not demonstrate a strong influence of the shape of the voltage pulse, the further experiment should be fulfilled.

8. Analysis of the time-history of the pumping and the laser pulses demonstrates that the EBCD itself strongly effects on laser characteristics. An inversion population and, hence, FO lasing itself take place in afterglow mode, as a rule. The experiments with crowbarred EBCD demonstrates that FO lasing is suppressed during the discharge. Therefore from one hand EBCD creates inversion population, from the other hand destroys it, perhaps, by the process of superelastic electron collisions.

4. Results of simulations in frames of the base model

For the set of parameters corresponding to the reference experimental data described in the section 3, some dependencies of the FO laser efficiency were computed using the base model described in the section 2. In particular, the dependence of the laser efficiency on the output coupling varied in experiments by rotation of the output plate (simultaneously it plays a role of the spectral filter) is shown in **Fig.**4.1. Curve 1 illustrates the efficiency predicted by our base model for experimental conditions, and the potentially available (when all useless losses are eliminated) laser efficiency is shown (curve 2). The achievement of this predicted high efficiency can be considered as a final aim of researches. For some not yet quite clear reasons, the experimental time of lasing delay relative to the discharge pulse is longer several times than predicted by our model. To estimate the role of this effect additional calculations were made in which the threshold cavity gain was kept as very high one up to the moment corresponding to the start of lasing in experiments. Then, at this moment the cavity threshold gain was set to be equal to that calculated from the total cavity losses (see **Fig.** 2.9). The result of these calculations is shown in **Fig.** 4.1 by the curve 3. It is seen that only this effect can not explain the experimental dependence.

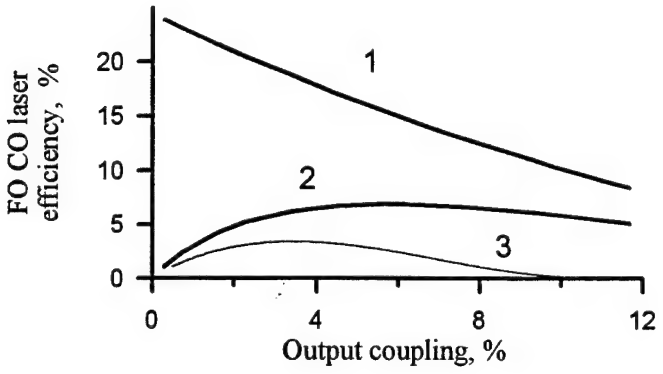

Fig. 4.1. Calculated laser efficiency vs output coupling of resonator:
$CO:N_2 = 1:9$;
$N = 0.3$ Amagat;
$T_0 = 105$ K;
$Q_{in} = 334$ J/l Amagat;
1- for ideal resonator without useless losses;
2- for measured cavity losses;
3- delay time as fit parameter was taken from experiment.

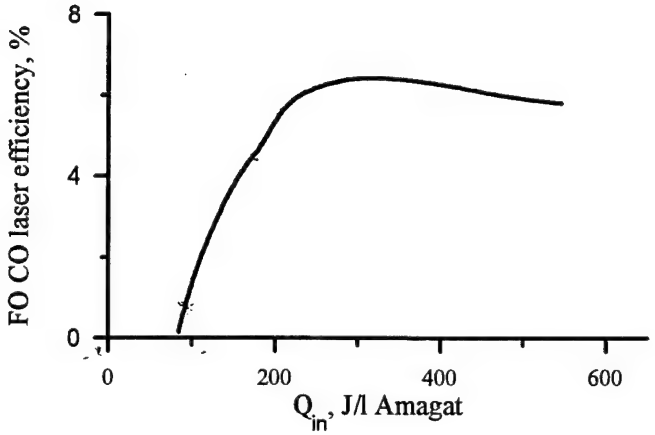

Fig. 4.2. Calculated laser efficiency as a function of specific input energy for the mixture
$CO:N_2 = 1:9$;
$N = 0.3$ Amagat;
$T_0 = 105$ K

Fig.4.2 demonstrates the dependence of the laser efficiency on the SIE Q_{in}. The predicted maximum takes place at Q_{in} = 300 J/l Amagat. The decrease of the laser efficiency for $Q_{in} > 300$ J/l Amagat is explained in our model by increasing the role of the energy redistribution between vibrations of CO and

N_2 . With time the more and more fraction of discharge power flows into the excitation of N_2 vibrations. The energy exchange between excited N_2 and CO is less effective and relatively slow resulting in diminishing the efficiency. Similar calculations were made for the laser mixture CO: N_2:He = 1:9:10. The result is shown in **Fig.**4.3. The optimum energy deposition in He-containing mixture is lower, and the magnitude of the laser efficiency is also diminished in comparison with CO: N_2 mixture.

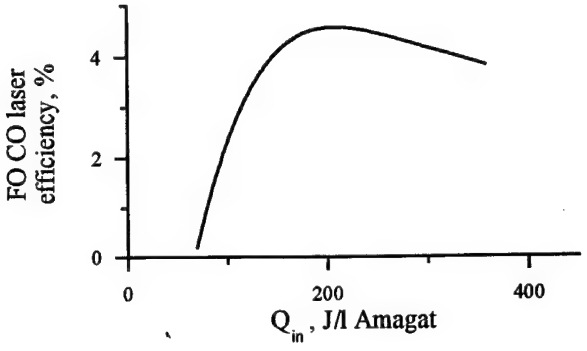

Fig.4.3. Calculated laser efficiency as a function of specific input energy for the mixture CO:N_2:He = 1:9:10; N = 0.3 Amagat; T_0 = 105 K

The accuracy of experimental estimations of the useless cavity losses is not very high. Therefore the study was made of the diverse influence of the useless optical losses on the laser efficiency. **Fig.**4.4 demonstrates how the calculated laser efficiency diminishes with growth of the additional useless losses. One can see that this influence is indeed quite strong. At the additional losses 18% lasing stops. The sensitivity of the laser efficiency to the increase of the gas temperature is illustrated in **Fig.**4.5. There are known several reasons for the efficiency to become lower with the temperature growth. First of all, this is an increase of the threshold vibrational energy after reaching of which the plateau in the VDF is formed. Other negative effects: accelerating of the V-T relaxation processes; shift to higher J values of the region where the partial inversion exists.

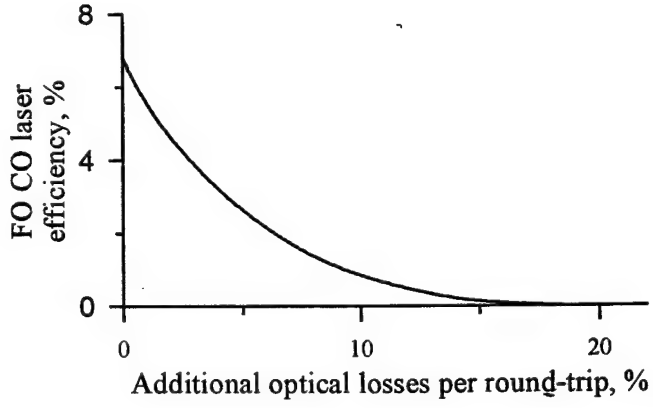

Fig. 4.4. Calculated laser efficiency vs additional optical losses of laser resonator; CO:N_2 = 1:9; N = 0.3 Amagat; T_0 = 105 K; Q_{in} = 334 J/l Amagat.

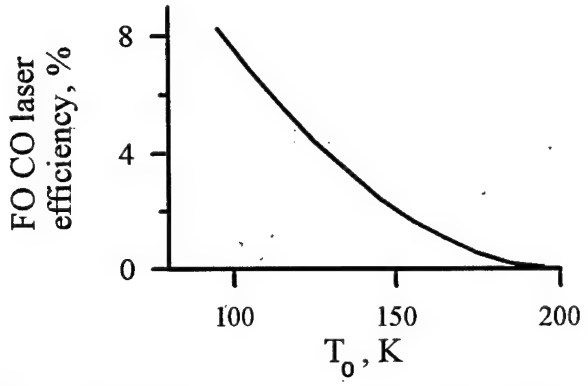

Fig. 4.5. Calculated dependence of laser efficiency on initial gas temperature;
CO:N_2 = 1:9;
N = 0.3 Amagat

As in experiments, studies were made on the role of the gas mixture composition. **Fig.**4.6 demonstrates computed variations of the laser efficiency associated with different concentration of N_2 in CO: N_2 mixture. Optimum concentration of N_2 is between 75 and 85%, while experimentally it was found to be 90%. In experiments the addition of He plays a positive role increasing in some limits the laser efficiency. Calculations predict that some improvement of laser efficiency is possible only for low concentration of He in the range 10-20% (see **Fig.**4.7). The further increase of the He fraction in the mixture CO: N_2 :He = 1:9:X is followed by diminishing the laser efficiency. In the theory, the positive role of He at low concentrations of it can be explained by some increase of the energy deposited per one CO molecule because the electron energy loss in collisions with He atoms is negligible. With further growth of He fraction, the theory predicts the decrease of the efficiency because of stronger V-T relaxation processes and CO vibration excitation degree becoming greater than the optimum one.

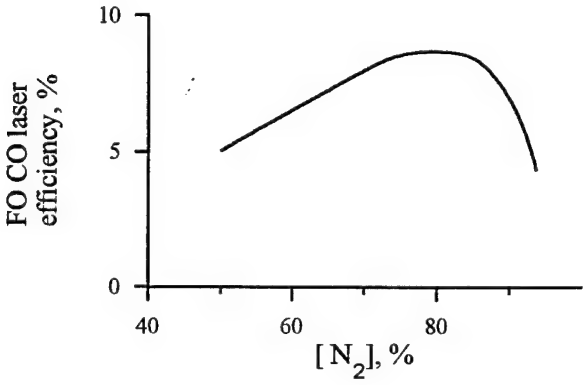

Fig.4.6. Calculated dependence of laser efficiency on nitrogen concentration in the mixture
CO:N_2 = 1:X;
N = 0.3 Amagat;
T_0 = 105 K;
Q_{in} = 334 J/l Amagat

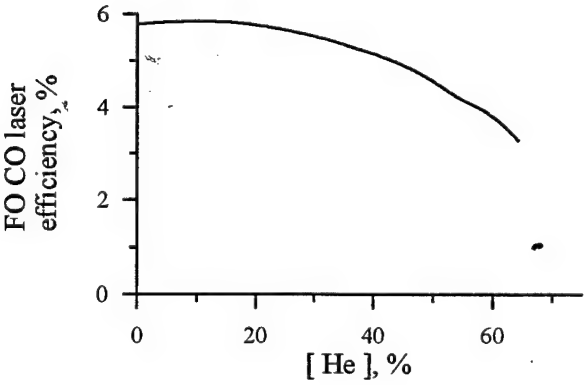

Fig.4.7. Calculated dependence of laser efficiency on He concentration in the mixture
CO:N_2:He = 1:9:X;
N = 0.3 Amagat;
T_0 = 105 K;
Q_{in} = 205 J/l Amagat

In this section the particular attention was paid to studies of parameter dependencies of the laser efficiency. This may be explained by an extreme importance of this information from the practical point of view. In fact, our model produced much more information than it was presented above. Comparing predicted parameter dependencies with experimental ones, strong discrepancies were observed in magnitude of the laser efficiency despite that special measures were undertaken the model to be as close to the experiment as possible. In this situation it would be helpful to look at the available information more thoroughly.

Fig.4.8 shows the predicted laser radiation spectrum calculated for the reference conditions. The most energy containing part of this spectrum corresponds to transitions from 11→9 to 16→14. This also disagrees with the experiment where the laser spectrum consists of transitions higher than 15→13. However, the strongest discrepancy is observed between calculated and experimentally detected waveform of the laser pulse. Curve 1 in **Fig.**4. 9 shows that the laser pulse delay relative to the discharge ignition is about 20 μs long and the duration of the pulse is of the order of 100 μs. Typical delay times observed in experiments are 50-70 μs, and the laser pulse duration is typically greater than 200 μs. In the next section an attempt is made to identify the reasons for these discrepancies, and results of some additional numerical studies are presented.

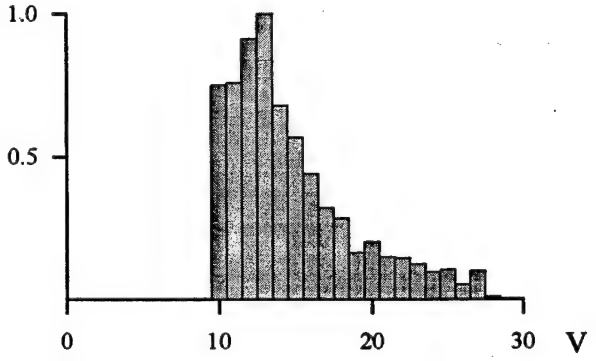

Fig. 4. 8. Calculated FO CO laser spectrum;
$CO:N_2 = 1:9$;
$N = 0.3$ Amagat;
$T_0 = 105$ K;
$Q_{in} = 364$ J/l Amagat

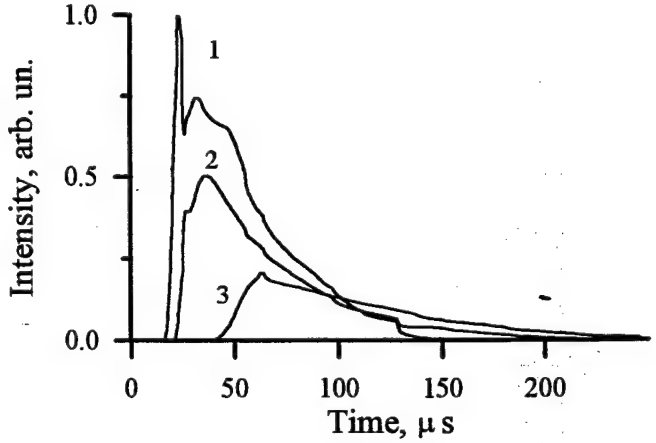

Fig. 4. 9. Calculated FO CO laser pulse waveform for different model assumptions
$CO:N_2 = 1:9$;
$N = 0.3$ Amagat;
$T_0 = 105$ K;
$Q_{in} = 364$ J/l Amagat):
1-base model;
2-absorption by atmospheric water vapor is taken into account;
3- water vapor absorption is included and enhanced discharge energy fraction for vibrational excitation of N_2 is taken into account.

5. Comparative analysis of experiment and theory, modifications of the model

To discuss how the theory and experiment agree each other a direct comparison of some theoretical and experimental results are presented here. Starting from the reference point described in **Table** 3.1, **Fig.**5.1 shows the dependence of the FO CO laser efficiency on the output coupling. In this figure the computed results presented above in **Fig.**4.1 are compared with the experimental data corresponding to **Fig.**3.9. Our base model overestimates the laser efficiency more than 3 times. Similar situation takes place when comparing measured and computed dependencies of the laser efficiency on the SIE for both He-free (see **Fig.**5.2) and He-containing mixtures (**Fig.**5.3). The disagreement is not so strong for the mixture with 50% of He. However, not only a magnitude of the laser efficiency, but the position of the optimum efficiency differs, too: 200 J/l Amagat in the theory vs 350 J/l Amagat in the experiment.

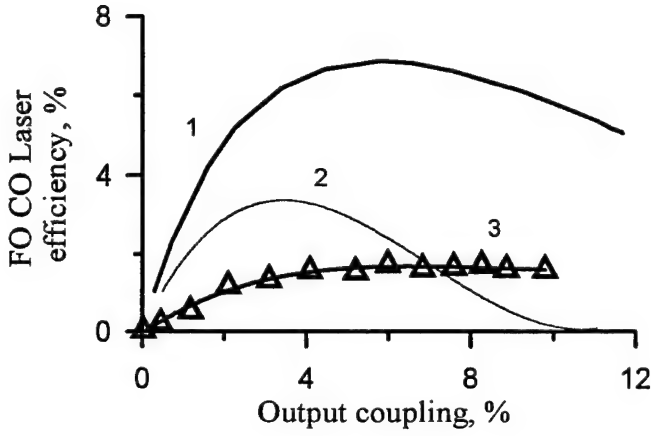

Fig.5.1. FO CO laser efficiency vs output coupling of the laser resonator.
$CO:N_2 = 1:9$;
$N = 0.3$ Amagat;
$T_0 = 105$ K.
Theoretical results for
$Q_{in} = 334$ J/l Amagat.
1 - for measured cavity losses;
2 - delay time as fit parameter was taken from experiment.
3 - Experimental data for
$Q_{in} = 300$ J/l Amagat.

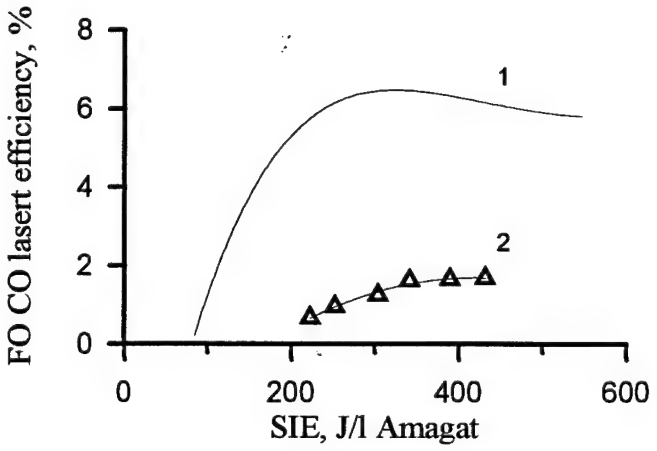

Fig.5.2. FO CO laser efficiency vs SIE for gas mixture
$CO:N_2 = 1:9$;
$N = 0.3$ Amagat;
$T_0 = 105$ K.
1 - Theory;
2 - Experiment.

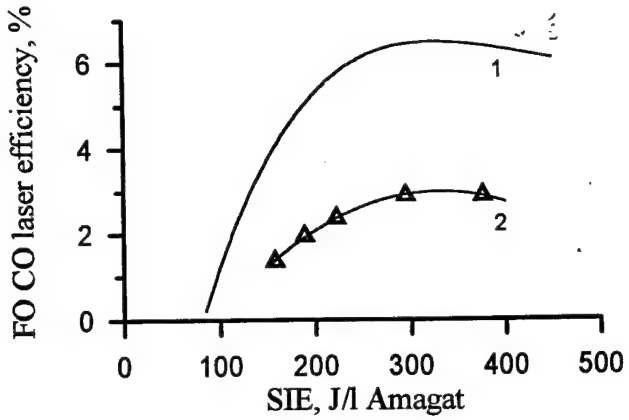

Fig.5.3. FO CO laser efficiency vs SIE for gas mixture $CO:N_2:He = 1:9:10$; $N = 0.3$ Amagat; $T_0 = 105$ K.
1 - Theory;
2 - Experiment.

When comparing the dependence of the laser efficiency on the additional optical losses shown in **Fig.**5.4 it can be seen that the differences between the experiment and the theory stem from overestimation of the active medium gain by the theory (this agrees with discussed above discrepancies in the laser efficiency). Predicted by the theory laser efficiency keeps to be higher in the all range of gas temperature variation realised in the experiment as shown in **Fig.**5.5.

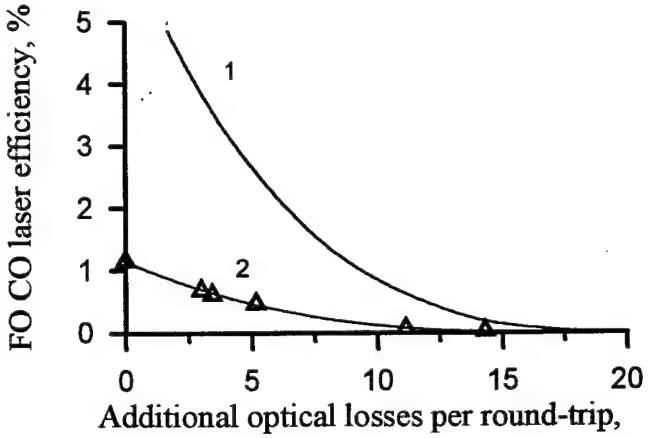

Fig.5.4. FO CO laser efficiency vs additional optical losses of resonator;
$CO:N_2 = 1:9$;
$N = 0.3$ Amagat;
$T_0 = 105$ K;
1 - Theory ($Q_{in} = 334$ J/l Amagat).;
2 - Experiment ($Q_{in} = 300$ J/l Amagat; diameter of laser aperture 20 mm and $V_{las} = 0.4$ l).

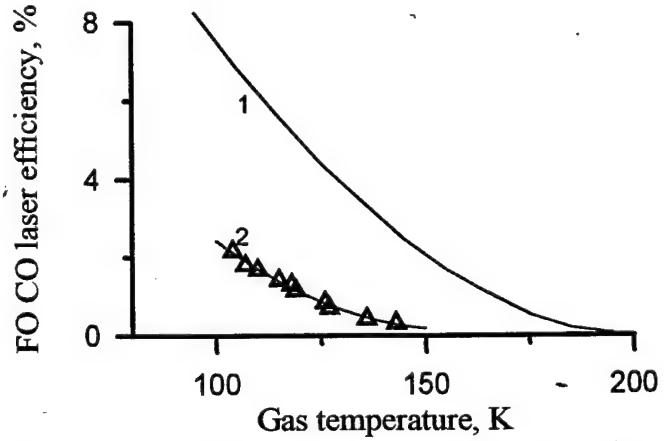

Fig.5.5. FO CO laser efficiency vs initial gas temperature.
$CO:N_2 = 1:9$;
$N = 0.3$ Amagat;
$Q_{in} = 330$ J/l Amagat
1 - Theory;
2 - Experiment.

The dependence of the FO CO laser efficiency on the gas composition observed in the experiments and calculated in the theory is illustrated by **Fig.**5.6 and 5.7. Ignoring the noted above disagreement in magnitude of the efficiency, the predicted dependence on the N_2 fraction is similar to the observed one. The experimental optimum N_2 concentration is higher (90%) but not so much (in theory between 75-

85%). The discrepancy between the calculated and measured dependencies on He fraction is stronger: the predicted optimum He concentration is 20% vs the experimental value 50% (see **Fig.**5.7). This discrepancy can be explained by a positive role of He in experiments associated with increasing of a thermal diffusion coefficient for He-containing mixtures. In an experimental construction some temperature gradients may exist directed to the bottom and hence not exciting gas convection . In this situation the molecular thermal diffusion becomes important influencing on the average gas temperature.

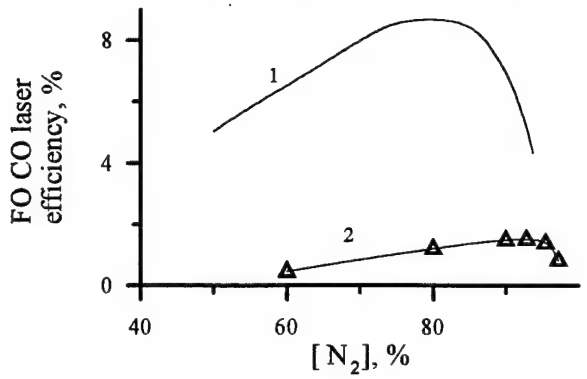

Fig.5.6. FO CO laser efficiency vs nitrogen concentration in the gas mixture $CO:N_2 = 1:X$;
$N = 0.3$ Amagat;
$T_0 = 105$ K.
1 - Theory
$Q_{in} = 334$ J/l Amagat.
2 - Experiment
$Q_{in} = 300$ J/l Amagat.

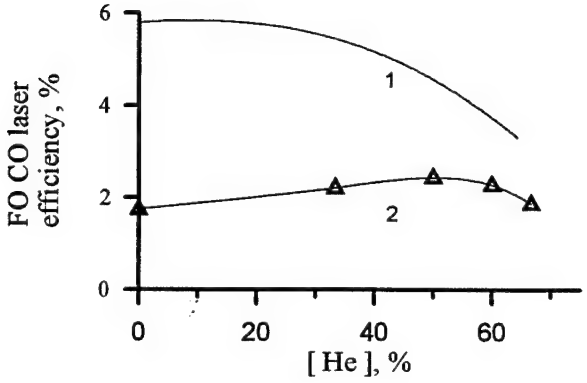

Fig.5.7. FO CO laser efficiency vs helium concentration in gas mixture $CO:N_2:He = 1:9:X$;
$N = 0.3$ Amagat;
$T_0 = 105$ K.
1 - Theory
$Q_{in} = 205$ J/l Amagat.
2 - Experiment
$Q_{in} = 300$ J/l Amagat.

A comparison of the experimental results with the theoretical predictions allows us to draw a conclusion that the theory more or less satisfactorily describes general trends observed in the experiments. However, the magnitude of a number of physical quantities strongly differs from the experimental values: (1) the predicted laser efficiency is higher 1.5-3 times than experimental one, as a rule; (2) the predicted laser radiation spectrum contains strong spectral lines corresponding to vibrational-rotational transitions lower (shorter wavelengths) than observed in the experiments; (3) the delay time of the laser pulse calculated is shorter 3-4 times than experimental one; (4) the laser pulse duration is shorter than in the experiments, as a rule. These discrepancies do not allow us to use the model for reliable predictions of the FO CO laser characteristics. The analysis is necessary to perform to find the sources of the listed above differences.

From the results of the numerical simulations it is clear that the laser efficiency can be easily fitted to the experimental values simply by an introduction of the additional optical losses (see **Fig.**4.4). However, as laser spectrum as time dependencies of the laser pulse turned out to be much more stable, and can not be

fitted in this way to the experimental values. An attempt to use the laser pulse delay time as a parameter taken from the experiment demonstrates that the efficiency becomes of the order of the experimental one. However, its dependence on the output coupling is still quite far from the experimental one (**Fig.**5.1). It means that the processes leading to lengthening of the pulse delay should be described more correctly.

Comparing the measured (**Fig.**3.3) and computed (**Fig.**4.8) laser spectrum an idea arises that the difference between them might be explained by an absorption of laser radiation in an intracavity region occupied by atmospheric air. The length of this region in experiments was 25 cm. To evaluate this effect special measurements of atmospheric absorption spectrum were made for the wavelength range of interest for the FO CO laser. The absolute values of the atmosphere absorption coefficient were determined using the IR spectrophotometer PE -983G. For the measurements two channels were used: in a sample channel an additional path in ambient air with length 31 cm was introduced in comparison with the reference channel. The absorption spectrum was measured with the highest available resolution ~1 cm^{-1}. In air the following parameters were controlled: relative humidity; temperature and pressure. To detect the absorption by water vapour, in similar conditions and with the same diagnostic device the measurements were repeated but when the sample channel was blown off by dry nitrogen (water vapor content less than 15 ppm). Detracting the second absorption spectrum from the first one the absorption by water vapor was obtained. In this way the possible sources for errors like not exact balance of channels and distortions introduced by additional optical elements are eliminated. The absolute absorption data were used for calculations of the transmission spectrum through 1m-long atmosphere path. This spectrum is shown in **Fig.**5.8 for the relative humidity of air 20% at the temperature 20°C and pressure 747 Torr. The concentration of the water at these conditions is equal to 0.42% (the molecule number density $1.07\ 10^{17}$ cm^{-3}). The absorption coefficients in air for a large number of overtone transitions were found from these data.

It occurs that the dependence of the absorption coefficient on the number of the rotational component of P-branch is non-monotonous. Due to this fact some modernization of the numerical code was done allowing for calculation of the threshold coefficients for a great number of optical transitions. When calculating the time evolution of the laser spectrum the spectral lines were selected which have the largest difference between its gain at the moment and its threshold gain. The resulting laser spectrum, calculated in this manner for the same conditions as in **Fig.**4.8, is shown in **Fig.**5.9. Comparing both computed spectra with the experimental one (**Fig.**3.3) it can be seen that the agreement now, after the water vapor absorption was taken into account, becomes much better. At a present stage of measuring it may be considered as quite satisfactory.

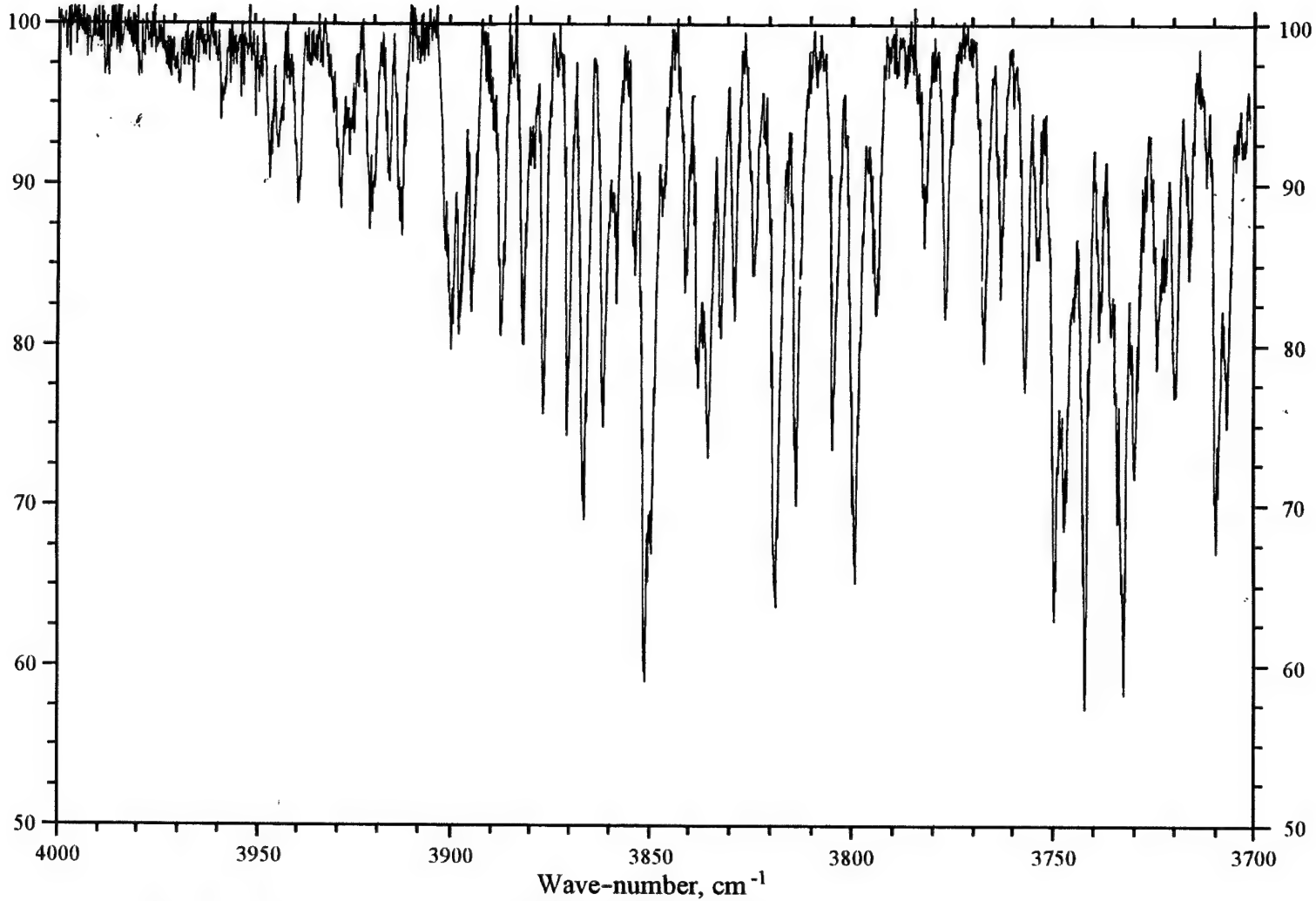

Fig.5.8a. Atmosphere transmittance (% m^{-1}) vs frequency of radiation. Relative humidity 20%, temperature 18oC, pressure 747 Torr.

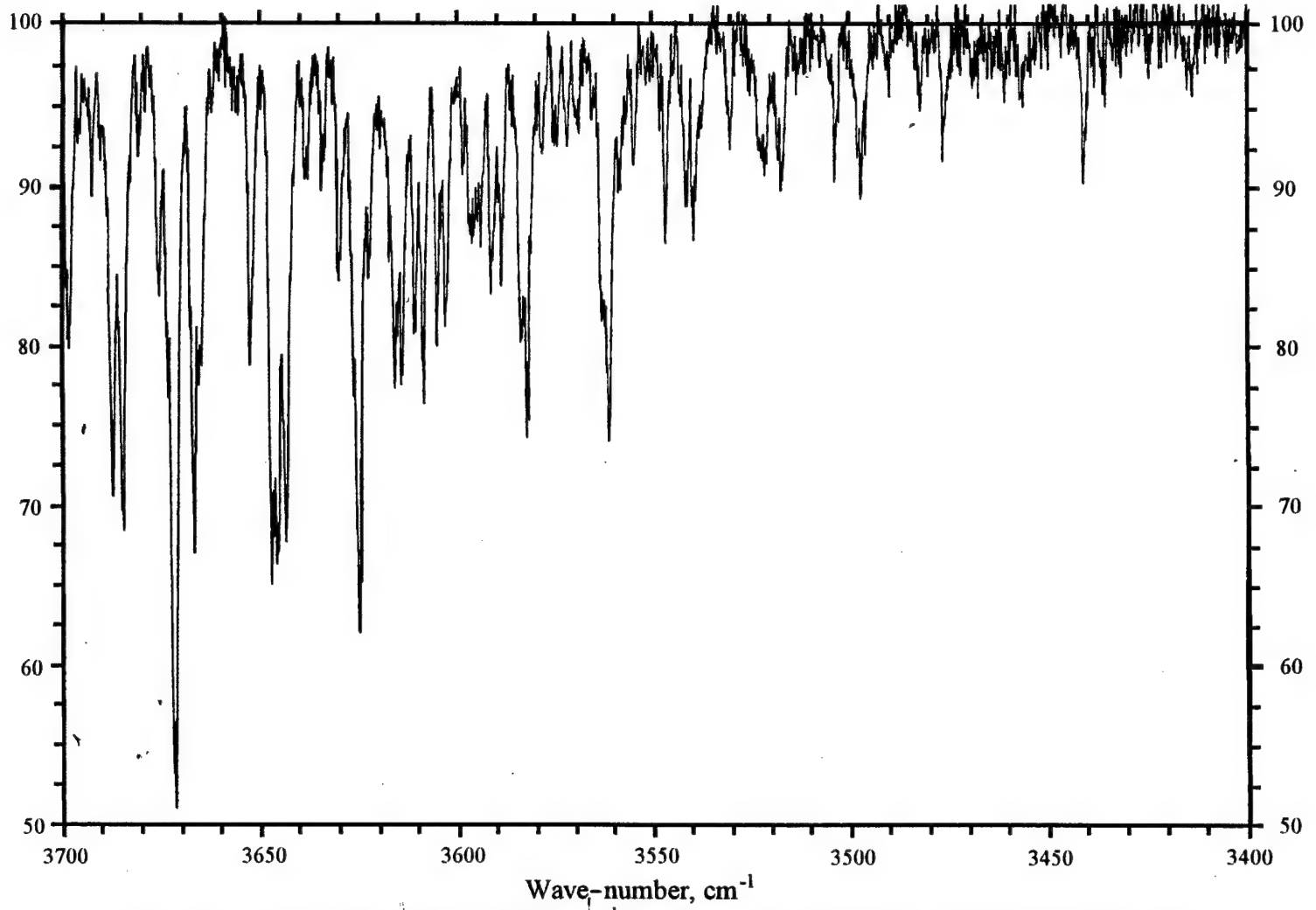

Fig.5.8b. Atmosphere transmittance (% m^{-1}) vs frequency of radiation. Relative humidity 20%, temperature 18oC, pressure 747 Torr.

Increasing cavity losses due to water vapor absorption leads automatically to the increase of the delay time (from 14.8 μs to 21.1 μs) and decrease of the laser efficiency (from 6.9% to 4.08%). The waveform of the laser pulse computed with water vapor absorption included is illustrated in **Fig.**4.9 by curve 2. Strong effect produced by absorption of the FO lines in atmospheric air should be necessarily taken into account in modeling.

It should be noted that disagreement between theory and experiment becomes less but still remains, in particular, in values of the delay time and pulse duration. At present, the effect of the atmosphere air absorption is described not quite accurately. In experiments there was no control of the air humidity and temperature. Therefore the air absorption in laser cavity was computed from the results of special measurements in an assumption of equal concentrations of the water vapor in both cases. For more accurate comparison the humidity and temperature in the room where the laser facility is placed should be measured. Spectrophotometric measurements showed that the atmosphere transmission varies with both: air humidity and temperature. In certain conditions the absorption by water molecular clusters was detected. Due to cluster absorption the change of the transmission coefficient is spectrally dependent leading to complicated variations in the spectrum of the threshold coefficients. This effect also demands that the state of the atmosphere in work room should be characterized carefully.

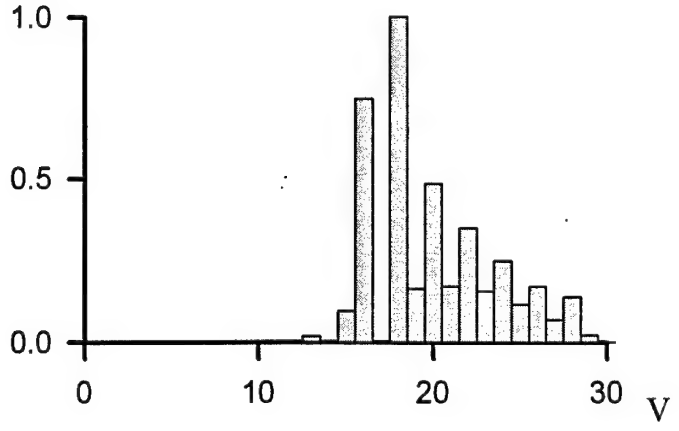

Fig.5.9. Overtone laser spectrum calculated taking into account the atmospheric water vapor absorption:
$CO:N_2 = 1:9$;
$N = 0.3$ Amagat;
$T_0 = 105$ K;
$Q_{in} = 364$ J/l Amagat.

The remaining disagreement is still strong stimulating further search of reasons for this. As was mentioned above, the delay time for the laser pulse being shorter than in the experiments is stable against variation of many parameters. Special numerical studies showed that starting from the reference point variation of the SIE from 330 L/l Amagat down to 140 J/l Amagat was followed by growth of the delay time, τ, from 14.7 μs up to 23 μs. The increase of the initial gas temperature in the active medium up to 150 K gave $\tau = 32$ μs, and the increase of useless cavity losses on additional 10% per round-trip gave $\tau = 24$ μs. These variations of parameters are far beyond the possible errors, and the delay time is still less than in experiments.

The next assumption attempting to explain this disagreement was about the negative role which may play the edges of the discharge region where the input power diminishes to zero. The idea is that to the moment of lasing a region exists with the lower input power having absorption induced by excitation in the discharge instead of gain. **Fig.** 5.10 illustrates time evolution of the absorption/gain coefficient at the potentially lasing transitions for the region with the low value of the SIE, Q_{in} = 45 J/l Amagat. It can be seen that the absorption coefficient magnitude is low, and to the moment of experimental pulse begining (~50 μs) the absorption disappeared. Hence this mechanism of increasing of the delay time seems to be improbable in the conditions of the experiments.

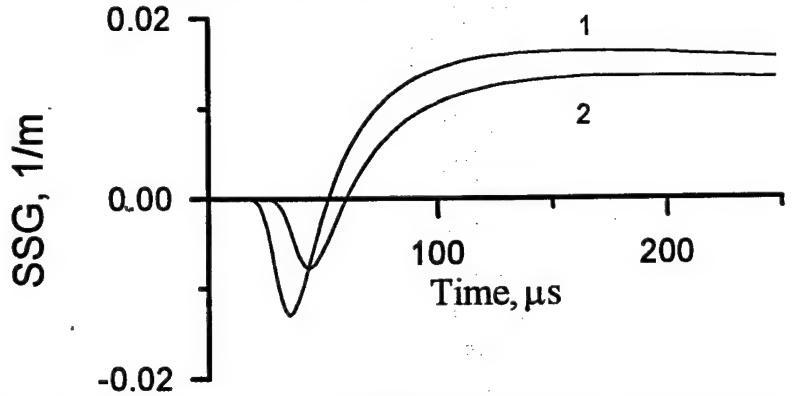

Fig.5.10. The absorption/gain coefficients vs time for transitions P(16, 12), P(18, 13): $CO:N_2$ = 1:9; N = 0.3 Amagat; T_0 = 105 K; Q_{in} = 45 J/l Amagat

One more assumption about mechanism governing such a long delay time as observed in the experiments was tested numerically. As it was discussed in the section 2.2.4 the electron scattering cross sections from vibrational excited molecules of N_2 and CO were never measured, and the accuracy of theoretical quantum mechanical calculations is not known. However, in conditions typical for the FO CO laser the role of vibrational excited molecules is even greater than for the FB CO laser. **Fig.**5.11 illustrates how electron collisions with excited molecules influence on the time evolution of the energy balance in the discharge. The redistribution of energy between CO and N_2 is due only to the effect of electron collisions with excited molecules. It can be seen, that initially going to vibrations of CO molecules fraction of pumping energy later goes preferentially to vibrations of N_2. Because of variation with time of the input power and parameter E/N **Fig.**5.12 gives better understanding of discussed effects showing how the electric power fractions going to excitation of CO and N_2 vibrations vary with time. To check the sensitivity of this effect to the magnitude of the electron scattering cross sections calculations were performed for two sets of cross sections differing only by maximum amplitude about 1.5 times. It can be seen that the energy redistribution effect is insensitive to the amplitude of cross sections.

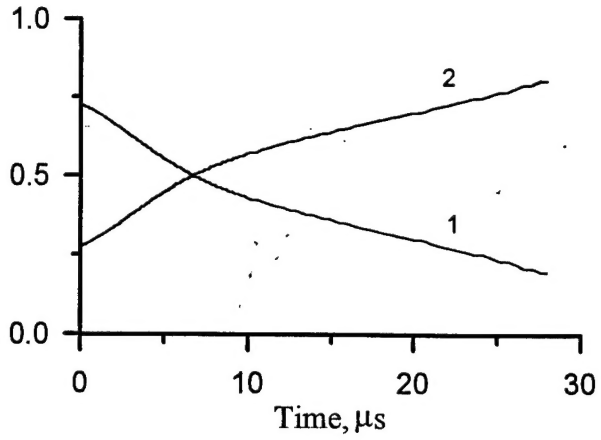

Fig.5.11. Variation of relative partitioning of input power between CO and N_2 vibrations in time:
CO:N_2=1:9;
N = 0.3 Amagat;
T_0 = 105 K;
Q_{in} = 364 J/l Amagat.
1 -fraction going to vibrations of CO;
2- fraction going to vibrations of N_2.

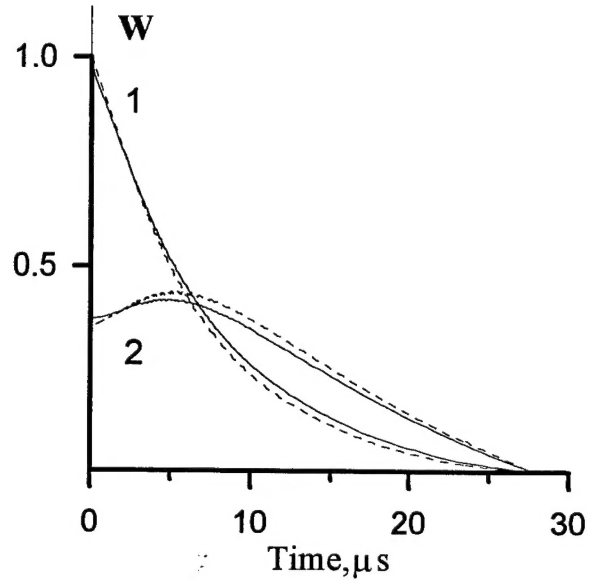

Fig.5.12. Variations of discharge power fractions going to vibrational excitation of CO and N_2 molecules with time:
1 - CO;
2 - N_2;
solid lines - old cross sections;
dashed lines - new set of vibrational excitation cross sections

However, one may expect that the discussed effect of the energy redistribution is much more sensitive to variations of electron scattering cross sections from vibrational excited molecules. Trying to estimate a possible effect, we change the energy balance in a simple way: the energy fraction going to vibrations of N_2 was increased by 19% relatively to what was calculated from the Boltzmann equation. The laser pulse waveform calculated in this approximation is shown by curve 3 in **Fig.**4.9. The pulse delay time and duration, both increase and become close to the experimental values. The computed laser efficiency is 2.3%.

Results of the last calculations may be considered as an indication to the possibility to improve modeling by critical studying of existing data about electron scattering from vibrational excited molecules.

6. Conclusions

Experimental and theoretical parametric study of FO CO laser with suppressed FB CO lasing has been carried out. FO CO lasing took place from 13→11 up to 25→23 vibrational transitions (λ=2.7-3.3 μm). The maximum SSG measured in the experiments was 0.14 m^{-1}. The optimal equivalent output coupling at given SSG, active length and optical losses lay at the range of 4-10%. The maximum FO CO laser efficiency was 3%. When decreasing useless optical losses from 12% per round-trip in the experiment down to 3% in future, expected laser efficiency could be 10%.

The developed earlier numerical model (Belykh et al, 1994, 1995) was adapted to the present experimental conditions and used for calculations of parameter dependencies of the FO CO laser efficiency. It turned out that theoretical predictions in frames of this base model differ strongly from the experiment. Explanation, why there was a good agreement with earlier experiments (Belykh et al, 1994, 1995) and now it is not so good, lies probably in differences in experimental conditions in (Belykh et al, 1994, 1995) and present ones. The most important differences are in pumping pulse duration (1.5 μs vs. ≥25 μs) and parameter *E/N* governing the excitation efficiency ((5-6) 10^{-16} V cm^2 vs. (1-2) 10^{-16} V cm^2). It seems that our model needs not to be modified for conditions of more intense pumping.

While the theory predicts more or less correctly general parameter dependencies, there are discrepancies in magnitudes of the laser efficiency, small signal gain, laser pulse delay time and laser pulse duration. Additional studies allow us to find one factor, earlier ignored, having a strong impact on the laser characteristics in experimental conditions: absorption by atmospheric air which is due to the presence of water vapor mostly. From the other side, it was shown numerically that the edge discharge non-uniformity can not be the reason for strong disagreement between the experiment and the theory.

To remove remaining discrepancies it is necessary to carry out additional studies. At the moment several factors can be pointed out, the influence of which on the FO CO laser characteristics should be studied experimentally and/or theoretically:

- a fraction of electron energy released in heating of gas in discharge (theoretical fit parameter taken here to be equal to 15%);
- a set of electron scattering cross sections for a manifold of vibrational levels $1 \le v \le 8$ of CO and N_2;
- exact ambient air parameters (humidity and temperature);
- EBCD characteristics.

The last point should be commented. For low-density-current (≤ 100 μA/cm^2) electron beam it was shown (Napartovich, 1996) that characteristics of the EBCD are very sensitive to the presence of

electronegative additives with low concentrations. For our conditions the role of small concentration additives should be studied also. The aim of the discharge studies would be an identification of mechanisms of instabilities restricting the discharge input power.

Therefore the further efforts should be aimed at fitting the theory to experiments and an increase of experimental laser efficiency. The possible ways of increasing the latter could be as follows:

- A decrease of useless optical losses in the laser resonator. An absorption of the spectral filter should and could be diminished by using the thinner one . The development of such a filter is under way at the moment. The better way is using special output coupler (with reflectivity 90-96% at 2.7-4.0 μm spectral region and reflectivity less than 0.5% at 4.9-6.0 μm) and totally reflected mirror with interference coating ($r = 99.9\%$, $\lambda = 2.7\text{-}4.0$ μm; $r \leq 0.5\%$, $\lambda = 4.9\text{-}6.0$ μm). Although the development of such kind of mirrors can face some difficulties.
- The placement of the mirrors on the laser chamber prevents also FO CO lasing from absorption by water vapor, that results in widening laser spectrum and increasing laser efficiency. However, the water vapor could operate as a spectral selector tuning the FO CO laser spectrum to the atmospheric transparency windows automatically, that can be extremely important for propagation of FO CO laser radiation through the atmosphere.
- A decrease of gas temperature. Supersonic expansion technique can be used for further cooling down the laser mixture. Special research should be done on supersonic laser facility.
- Shortening pumping pulse and its profile closer to rectangular one, an increase of an initial discharge voltage, perhaps, will lead to the increase of the laser efficiency.
- A purification of gas mixture component (carbon monoxide especially) could lead to an elimination of ingredients, which might depopulate the vibrational levels of N_2 and CO molecules.

7. References

Aleksandrov, N. L., Konchakov, A. M., Son, E. E., 1978, Fizika Plasmy, v. 5, 1182

Aleksandrov N.L., Konchakov A.M., Son E.E., 1979, Zhurnal Tekhnicheskoi Fiziki, v. 49, 1200

Allen D.C., Price T.J., Simpson C.J.S.M., 1980, Chemical Physics, v. 45, pp. 203-211

Andrews, A. J., Simpson, C. J. S. M., 1975, Chem. Phys. Lett., v. 36, 271

Andrews A.J., Simpson C.J.S.M., 1984, Chemical Physics, v. 64, pp. 299-311

Bachem E., Dax A., Fink T. et al, 1993, Appl. Phys. v.B57, 185.

Basov N.G., Danilychev V.A., Ionin A.A. et al, 1978, Kvantovaya Electronika, v.5 ,1855.

Basov N.G., Kazakevich V.S., Kovsh I.B., 1980a, Kvantovaya Electronika, v.7, 1966.

Basov N.G., Kazakevich V.S., Kovsh I.B., 1980b, Kvantovaya Electronika, v.7, 1973.

Basov N.G., Danilychev V.A., Ionin A.A. Kovsh I.B., 1980c, J. Sov.Laser Research, v.1, N4, 311-349.

Basov N.G., Bakaev V.G., Ionin A.A. et al, 1983, Kvantovaya Elektronika, v. 10, 1261

Basov N.G., Ionin A.A., Kovsh I.B., 1985, Infrared Physics, v.25, 47.

Belykh A.D., Gurashvili V.A., Kochetov I.V., Kurnosov A.K., Napartovich A.P., Putilin V.M., 1994, Pulsed CO overtone laser: theory and experiment. SPIE Proceedings, **2117**, #14,12

Belykh A.D., Gurashvili V.A., Napartovich A.P. et al, 1995, Kvantovaya Electronika, v.22, 333.

Berdyshev A.V., Kochetov I.V., Napartovich A.P., 1988, Khimicheskaya Fizika, v. 7, 470

Bergman R.C., Rich J.W., 1977, Appl.Phys.Lett. v.31, 597.

Billing G.D., Fisher E.R., 1979, Chemical Physics, v.,43, pp.,395-401

Billing G.D., 1980, Chemical Physics, v. 50, pp. 165-173

Billing G.D., Cacciatore M., 1983, Chem. Phys. Lett., v. 94, 218

Bounich J.P., Brodbeck C., 1973, J. Quant. Spectr. & Rad. Transfer, v. 13, 1

Farrenq R, Rosetti C., Guelachvili G., Urban W., 1985, Chemical Physics, v. 92, 389

Flament C., George T., Meister K.A. et al., 1992, Chemical Physics, v. 163, pp. 241-262

Gromoll-Bohle M., Bohle W., Urban W., 1989, Opt. Comm., v.69, 409.

Guelachvili G., Villeneuve D., Farrrenq R. et al, 1983, J. Mol. Spectr., v. 98, 64

Herzfeld K.F., Litovitz, 1959, Absorption and Dispersion of Ultrasonic Waves, N.Y.

Hunt R.H., Toth R.A., Plyler E.K., 1968, J. Chem. Phys., v. 49, 3909

Ionin A. and Spalding I., 1996a, "CO-lasers - state of the art and potential of applications" in "Gas Lasers - Recent Developments and Future Prospects", Ed. by W.J. Witteman and V.N. Ochkin, NATO ASI Series, 3. High Technology - Vol.1.10, pp. 279-289.

Ionin A., Galushkin M., Kotkov A., Mitin K. et al, 1996b, "Degenerate four-wave mixing and phase conjugation of molecular mid-IR lasers radiation in their inverted media," Scientific report of Lebedev Institute on Contract SPC-95-4043 with EOARD

Ichshenko E.F., Klimkov Yu.M., 1968, "Optical quantum generators," "Soviet Radio," Moscow

Islamov R.Sh., Konev Yu.B., Kochetov I.V., Kurnosov A.K., 1984, Kvantovaya Elektronika, v. 11, 142

Kochetov I.V., 1976, Thesis of candidate dissertation, Moscow Institute of Physics and Technology, Moscow

Konev Yu.B., Kochetov I.V., Kurnosov A.K., Pevgov V.G., 1977, Pis'ma v ZhTF, v. 3, 1267

Konev Yu.B., Kochetov I.V. et al, 1981, Inzhenerno Fizicheskii Zhurnal, v. 41, 514

Lightman A.J., Fisher E.R., 1978, J. Appl. Phys., v. 49, 971

Mastrocinque G., Chakroun A., Doyenette L. et al., 1976, Chemical Physics Letters, v.39, pp.347-349

Napartovich A.P., 1996, Physics of high-power CO laser, in "Gas Lasers-Recent Developments and Future Prospects", Ed. by W. J. Witteman and V. N. Ochkin, NATO ASI Series, 3. HighTechnology-Vol. 10

Patel C.K.N., 1964, Phys. Rev., v. 136A, 1187

Penner S.S., 1959, Quantitative molecular spectroscopy and gas emissivities, Addison-Wesley, Reading

Rapp D., Englander-Golden, P., 1964, Journal of Chemical Physics, v. 40, pp.573-575

Rockwood S.D., Bray J.E., Proctor W.A., Canavan, G.H., 1973, IEEE Journal of QE, v.,9, pp.,120-129

Schulz G.J., 1979, In: Electron Molecule Scattering, ed. S. C. Brown, Wiley, New York, Chap. 1

Sharma R.D., Brau C.A., 1969, J. Chem. Phys. v. 50, 924

Shin H.K., Altick P.L., 1977, Chemical Physics Letters, v.52, pp.580-586

Smith N.S., Hassan H.A., 1976, AIAA Journal, v. 14, pp.374-381

Stanton A.S., Hanson R.K., Mitchner M., 1980, J. of Appl. Phys., v. 51, pp.1360-1378

Treanor C.A., Rich I.W., Rehm R.G., 1968, J. Chem. Phys., v. 48, 1798

Zhdanok S.A., Napartovich A.P., Starostin A.N. 1979, Sov. Phys. JETP, v. 49, 66

Zhdanok S.A., Kochetov I.V. et al. 1988, Inzhenerno Fizicheskii Zhurnal, v. 38, 273